Article

7-Dehydrocholesterol is an endogenous suppressor of ferroptosis

https://doi.org/10.1038/s41586-023-06878-9

Received: 27 September 2021

Accepted: 17 November 2023

Published online: 31 January 2024

Check for updates

Florencio Porto Freitas[1,26], Hamed Alborzinia[2,3,26], Ancély Ferreira dos Santos[1,26], Palina Nepachalovich[4], Lohans Pedrera[5], Omkar Zilka[6], Alex Inague[1,7], Corinna Klein[2,3], Nesrine Aroua[2,3], Kamini Kaushal[2,3], Bettina Kast[2,3], Svenja M. Lorenz[8], Viktoria Kunz[9], Helene Nehring[1], Thamara N. Xavier da Silva[1], Zhiyi Chen[1], Sena Atici[1], Sebastian G. Doll[8], Emily L. Schaefer[6], Ifedapo Ekpo[6], Werner Schmitz[10], Aline Horling[11], Peter Imming[11], Sayuri Miyamoto[7], Ann M. Wehman[12], Thiago C. Genaro-Mattos[13], Karoly Mirnics[13], Lokender Kumar[14], Judith Klein-Seetharaman[15,16], Svenja Meierjohann[17], Isabel Weigand[18], Matthias Kroiss[18], Georg W. Bornkamm[19], Fernando Gomes[20], Luis Eduardo Soares Netto[20], Manjima B. Sathian[21], David B. Konrad[21], Douglas F. Covey[22,23], Bernhard Michalke[24], Kurt Bommert[9], Ralf C. Bargou[9], Ana Garcia-Saez[5], Derek A. Pratt[6], Maria Fedorova[4], Andreas Trumpp[2,3,25], Marcus Conrad[8] & José Pedro Friedmann Angeli[1]✉

Ferroptosis is a form of cell death that has received considerable attention not only as a means to eradicate defined tumour entities but also because it provides unforeseen insights into the metabolic adaptation that tumours exploit to counteract phospholipid oxidation[1,2]. Here, we identify proferroptotic activity of 7-dehydrocholesterol reductase (DHCR7) and an unexpected prosurvival function of its substrate, 7-dehydrocholesterol (7-DHC). Although previous studies suggested that high concentrations of 7-DHC are cytotoxic to developing neurons by favouring lipid peroxidation[3], we now show that 7-DHC accumulation confers a robust prosurvival function in cancer cells. Because of its far superior reactivity towards peroxyl radicals, 7-DHC effectively shields (phospho) lipids from autoxidation and subsequent fragmentation. We provide validation in neuroblastoma and Burkitt's lymphoma xenografts where we demonstrate that the accumulation of 7-DHC is capable of inducing a shift towards a ferroptosis-resistant state in these tumours ultimately resulting in a more aggressive phenotype. Conclusively, our findings provide compelling evidence of a yet-unrecognized antiferroptotic activity of 7-DHC as a cell-intrinsic mechanism that could be exploited by cancer cells to escape ferroptosis.

Lipid components of cellular membranes are constantly exposed to free radical species that are competent to trigger their degradation through an oxygen-dependent process[4]. This process broadly known as lipid peroxidation is primarily dictated by the propagation rate constants (k_p) of its lipidic elements, an intrinsic chemical feature unique to each of these components. The past few years have witnessed a surge of interest in understanding the cellular mechanisms that regulate lipid peroxidation as they have been associated as key determinants of a distinct non-apoptotic cell death modality, known as ferroptosis[5].

Early works have established the central role of the enzymatic activity of the selenoprotein glutathione peroxidase 4 (GPX4)[2,6] in suppressing the process of ferroptosis[7–9]. GPX4 is the sole enzyme in mammals capable of directly reducing a broad range of peroxidized lipids present in membranes[10,11]. GPX4 can be irreversibly inhibited by a series of alkylating small molecules, such as RSL3 and ML210

[1]Rudolf Virchow Center for Integrative and Translational Bioimaging, University of Würzburg, Würzburg, Germany. [2]Heidelberg Institute for Stem Cell Technology and Experimental Medicine (HI-STEM gGmbH), Heidelberg, Germany. [3]Division of Stem Cells and Cancer, German Cancer Research Center (DKFZ) and DKFZ-ZMBH Alliance, Heidelberg, Germany. [4]Center of Membrane Biochemistry and Lipid Research, University Hospital and Faculty of Medicine Carl Gustav Carus of TU Dresden, Dresden, Germany. [5]Institute of Genetics, CECAD, University of Cologne, Cologne, Germany. [6]Department of Chemistry & Biomolecular Sciences, University of Ottawa, Ottawa, Ontario, Canada. [7]Instituto de Química, Universidade de Sao Paulo, Sao Paulo, Brazil. [8]Institute of Metabolism and Cell Death, Helmholtz Zentrum München, Neuherberg, Germany. [9]Comprehensive Cancer Center Mainfranken, Universitätsklinikum Würzburg, Würzburg, Germany. [10]Department of Biochemistry and Molecular Biology, Theodor Boveri Institute, Biocenter, University of Würzburg, Würzburg, Germany. [11]Institute of Pharmacy, Martin Luther University Halle Wittenberg, Halle, Germany. [12]Department of Biological Sciences, University of Denver, Denver, CO, USA. [13]Munroe-Meyer Institute for Genetics and Rehabilitation, University of Nebraska Medical Center, Omaha, NE, USA. [14]Faculty of Applied Sciences and Biotechnology, Shoolini University, Himachal Pradesh, India. [15]Department of Physics, Colorado School of Mines, Golden, CO, USA. [16]School of Molecular Sciences, Arizona State University, Phoenix, AZ, USA. [17]Department of Pathology, University of Würzburg, Würzburg, Germany. [18]Medizinische Klinik und Poliklinik IV, Ludwig Maximillian University, Munich, Germany. [19]Institute of Experimental Cancer Research, University Hospital Ulm, Ulm, Germany. [20]Instituto de Biociências, Universidade de São Paulo, São Paulo, Brazil. [21]Department of Pharmacy, Ludwig Maximilian University of Munich, Munich, Germany. [22]Department of Developmental Biology, Washington University in St. Louis, St. Louis, MO, USA. [23]Taylor Family Institute for Innovative Psychiatric Research, Washington University, St. Louis, MO, USA. [24]Research Unit Analytical BioGeoChemistry, Helmholtz Center München (HMGU), Neuherberg, Germany. [25]German Cancer Consortium (DKTK), Heidelberg, Germany. [26]These authors contributed equally: Florencio Porto Freitas, Hamed Alborzinia, Ancély Ferreira dos Santos. ✉e-mail: pedro.angeli@uni-wuerzburg.de

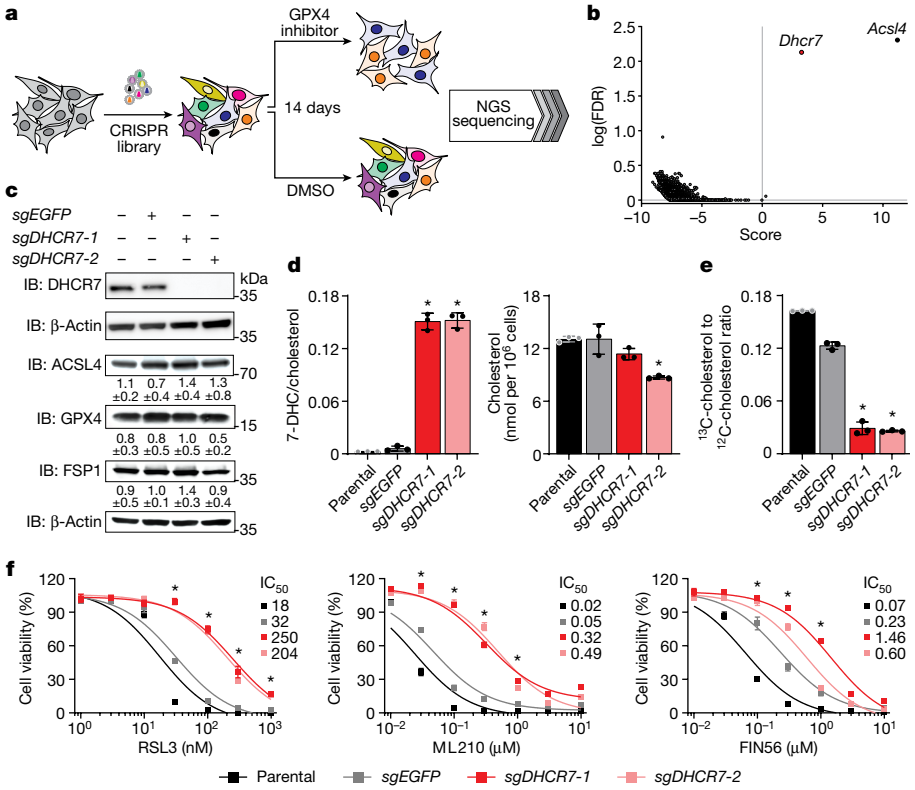

Fig. 1 | Identification and impact of DHCR7 deficiency on ferroptosis. **a**, Schematic of the identification of *Dhcr7* as a proferroptotic gene, using CRISPR-KO library and GPX4 inhibition. **b**, Volcano plot of sgRNA enriched in cells selected with RSL3 compared with untreated control cells. **c**, Immunoblot (IB) analysis of DHCR7 and key ferroptosis regulators, namely, FSP1, ACSL4 and GPX4 in cells expressing an sgRNA targeting *DHCR7* and *EGFP*. Values represent mean ± s.d. of ratio of protein of interest in relation to β-actin, $n = 3$ independent experiments. **d**, Relative quantification of 7-DHC and cholesterol concentrations in HT1080 cell lines stably transduced with a vector expressing Cas9 and a sgRNA targeting *DHCR7* and *EGFP* as a control. **e**, Assessment of de novo cholesterol biosynthesis, by means of the quantification of ^{13}C-cholesterol originating from ^{13}C-glucose in HT1080 cell expressing sgRNA targeting *DHCR7* and *EGFP* as control. Data are the mean ± s.d. of $n = 3$ wells of a 6-well plate from one representative experiment (**d**,**e**). **f**, Dose-dependent toxicity of the ferroptosis inducers RSL3, ML210 and FIN56 in HT1080 cell lines stably transduced with a vector expressing Cas9 and an sgRNA targeting *DHCR7* and *EGFP* as a control. Cell viability was monitored using Alamar blue after 48 h (**f**) and represented as the mean ± s.d. of triplicates from one representative of two independent experiments (**f**). *$P < 0.05$; two-way analysis of variance (ANOVA) (**d**–**f**).

(ref. 8), leading to cell death in ferroptosis-sensitive cancer cell lines. The enrichment of phospholipids with polyunsaturated fatty acids (PUFAs) results in a marked dependency on GPX4 activity[12,13]. This high-PUFA state was shown to be largely dependent on the activity of the enzyme acyl-CoA-synthetase long-chain family 4 (ACSL4), which is required for the critical step of PUFA activation[12]. Accordingly, the inhibition of GPX4 in ferroptosis-prone cell lines leads to the characteristic oxidation fingerprint entailing the accumulation of peroxidized products of phosphatidylethanolamine (PE) containing arachidonic acid and adrenic acid[14]. It has been further demonstrated that the sole accumulation of peroxidized fatty acids is not sufficient to induce ferroptosis and a central role of the free radical-mediated propagation step has been unambiguously demonstrated[15]. The propagation step of lipid peroxidation was shown to contribute to the formation of pore-like structures of ill-defined identity[16] that drive the osmotic lysis of the cells[17].

The present study uncovered and characterized a role for 7-dehydrocholesterol reductase (DHCR7) in the ferroptotic process. DHCR7 catalyses the final step in cholesterol biosynthesis and its inhibition leads to the accumulation of 7-dehydrocholesterol (7-DHC). Others[18] initially reported 7-DHC to accumulate in preputial gland tumours and whose function, at that time, was only assumed to be as a spare capacity for cholesterol synthesis. Subsequent studies characterized 7-DHC as the most oxidizable lipid ever reported and whose accumulation predisposes cells to lipid peroxidation[19]. By contrast, we now show that the accumulation of 7-DHC causes a paradoxical increased tolerance towards phospholipid peroxidation, thus providing a robust resistance to ferroptosis. Furthermore, the characterization of the protective effect of 7-DHC provided valuable insights into the distinction between lipid and phospholipid peroxidation in cell death processes. By demonstrating the accumulation of oxidatively truncated phospholipid species in ferroptotic cell death, we emphasize the crucial role of these species in the execution of ferroptosis. Together with the accompanying paper[20], our findings suggest that manipulating this pathway could be exploited to increase ferroptosis resistance to suppress ferroptosis in acute settings but also exploited by cancer cells to evade ferroptosis.

DHCR7 is a proferroptotic gene

Spurred by the still incomplete understanding of the ferroptotic process and the development of next-generation single guide RNAs (sgRNAs)[21], we performed a genome-wide reverse genetic CRISPR screen to identify genes that may confer robust protection against ferroptosis. To this end, the Pfa1 cell line[6] was transduced with a CRISPR library covering 18,424 genes with a total representation of 90,230 sgRNAs followed by a stringent selection for 14 days using 200 nM of the GPX4 inhibitor (1*S*,3*R*)-RSL3 (in the following referred to as RSL3) (Fig. 1a). Consistent with the results of ours and others previous screens, *Acsl4* emerged as the highest-scoring hit[12,13,22–24]. The second top-scoring gene was *Dhcr7* (Fig. 1b). The identification of *Dhcr7* as a potential proferroptotic gene was surprising in light of several studies indicating

that loss or inhibition of DHCR7 is associated with an increased susceptibility to lipid peroxidation[4,25], which, in principle, should lead to an increased susceptibility to ferroptosis[26]. Intrigued by this finding, we set out to explore the basis of this discovery. Using the bona fide ferroptosis fibrosarcoma cell line model HT1080, we generated polyclonal cultures of *DHCR7*-deficient cell lines using two independent sgRNAs. The successful loss of DHCR7 was validated by western blot and mirrored by the accumulation of its substrate 7-DHC (Fig. 1c,d) and impaired incorporation of C^{13}-glucose into cholesterol (Fig. 1e). Notably, cholesterol depletion was less pronounced, suggesting that a substantial fraction is directly taken up from the serum. Importantly, knockout of *DHCR7* did not concur in a marked alteration in the protein concentrations of known ferroptosis regulators (Fig. 1c) nor the phospholipid composition of cells (Extended Data Fig. 1a–c). Using these cellular models, we validated the screening results showing that *DHCR7*-deficient HT1080 cells present a marked resistance to ferroptosis (Fig. 1f). Similar results were obtained with three independent clonal cell lines derived from Pfa1, HT1080 and MDA-MB-435 cells, confirming the general impact of this system in specifically preventing ferroptosis (Extended Data Fig. 2a–d). Subsequent studies focused on the clonal cell line derived from the HT1080 *DHCR7* knockout (KO) pool (a detailed characterization of the genetic modification of these cells is provided in Extended Data Fig. 3a–d). Thereby, we could unequivocally demonstrate the proferroptotic activity of DHCR7 because the genetic reconstitution of *DHCR7* abolished 7-DHC concentrations and resensitized cells to ferroptosis without affecting the response of the cell to other cytotoxic agents (Extended Data Fig. 3e–g).

7-DHC is an antiferroptotic metabolite

In the penultimate step of the cholesterol biosynthesis pathway, lathosterol, through lathosterol oxidase (SC5D), is converted to 7-DHC, which, in turn, is reduced to cholesterol by DHCR7 in the final step of the pathway (Fig. 2a and Extended Data Fig. 4a). Several previous studies have pointed to a toxic effect of 7-DHC accumulation through its inherent propensity to autoxidize and propagate radical chain reactions within the lipid bilayer[25]. To shed light on these seemingly paradoxical observations, we generated a *DHCR7 SC5D* double-mutant cell line to address whether 7-DHC accumulation mediates the protective effects induced by the loss of *DHCR7*. In agreement with a protective effect of 7-DHC, the loss of *SC5D* in the *DHCR7* KO cell line completely abolished the resistance conferred by the single loss of *DHCR7* (Fig. 2b). Similarly, pharmacological inhibition of upstream steps of cholesterol biosynthesis recapitulated this effect (Extended Data Fig. 4b). Accordingly, combined loss of *DHCR7* and *SC5D* led to a detectable accumulation of lathosterol and suppressed 7-DHC accumulation (Fig. 2c). Subsequently, the serial reconstitution of *DHCR7* and *SC5D* in a *DHCR7 SC5D* KO background demonstrated that the re-expression of *SC5D* resulted in substantial accumulation of 7-DHC as also validated by monitoring C^{13}-labelled glucose incorporation into 7-DHC and cholesterol (Fig. 2d,e,f). This, in turn, resulted in a specific increased resistance to ferroptosis (Fig. 2g and Extended Data Fig. 4c). Using wild-type (WT), *DHCR7* and *DHCR7 SC5D*-deficient cell lines in a series of sterol supplementation experiments, we further demonstrated that exogenous supplementation of 7-DHC protected all cell lines from ferroptosis; also, lathosterol only increased ferroptosis resistance in cell lines able to produce 7-DHC (Fig. 2h). Similar observations were made in the sgRNA expressing polyclonal cell population, where we could also demonstrate that squalene, a previously reported ferroptosis suppressor[27], failed to inhibit cell death when supplemented exogenously (Extended Data Fig. 4d). Importantly, a similar protective effect of 7-DHC was observed in a genetic model of *Gpx4* deficiency[6] (Extended Data Fig. 4e). Curiously, free cholesterol blunted the protective effects in all genotypes (Fig. 2h, and Extended Data Fig. 4f). Building on this observation we could show that an enantiomer of cholesterol, which has an opposite three-dimensional structure but identical physical properties to cholesterol[28], was markedly less efficient at blunting these protective effects (Extended Data Fig. 4g). Combined with the observed loss of 7-DHC in cells treated with free cholesterol (Extended Data Fig. 4h,i) our observations suggest an inhibitory effect on SREBP2 and biosynthetic activity of the mevalonate pathway.

Given the suppressive function of cholesterol on the protective effect conferred by 7-DHC, we investigated the response to ferroptosis in settings where cholesterol supply is scarce. To accomplish this, we cultivated cells in delipidated fetal bovine serum (dlFBS), which effectively removes sterols from the culture medium (Extended Data Fig. 5a). In dlFBS, we noted a decline in total cholesterol concentrations and a concurrent increase in 7-DHC in DHCR7-deficient cells, indicating enhanced biosynthesis (Extended Data Fig. 5b). Under this experimental condition, we consistently observed similar responses, albeit with heightened sensitivity, which can probably be attributed to reduced expression of GPX4 resulting from the fumed silica treatment (Extended Data Fig. 5c,d). Notably, the loss of GPX4 seems to be independent of sterol concentrations and is probably due to selenium depletion (Extended Data Fig. 5e,f). To mitigate potential confounding factors, we investigated the impact of LDL-receptor (LDLR) KO (Extended Data Fig. 5g). As anticipated, the KO cells exhibited increased expression of SREBP2 target genes, no differences in GPX4 concentrations and an inability to efficiently internalize fluorescently labelled LDL (Extended Data Fig. 5h–k). Treatment with the EBP inhibitor Tasin-1 induced a substantial reduction in cholesterol concentrations in the LDLR KO cells, whereas the WT cells remained largely unaffected (Extended Data Fig. 5l). Using these models, we show that the loss of LDLR does not significantly affect ferroptosis under normal conditions but pretreatment with Tasin-1 markedly sensitizes *LDLR* KO cells to ferroptosis (Extended Data Fig. 5m). These findings substantiate the notion that 7-DHC plays a crucial role in cellular protection, particularly in conditions where biosynthesis is stimulated.

7-DHC blocks phospholipid peroxidation

The conjugated double-bond present in the sterol B-ring stands as the most prominent feature of 7-DHC, when compared to the other sterols. To probe the relevance of this feature in preventing ferroptosis we assayed the structurally related sterol ergosterol for its capacity to supress ferroptosis (Extended Data Fig. 6a) and showed that it has an equally potent antiferroptotic activity (Extended Data Fig. 6b). Given that ergosterol is the main sterol component in yeast and fungi, it was reasonable to assume that this lipid could be an important suppressor of cell death induced by PUFAs in these evolutionarily distant organisms. In fact, we could validate this hypothesis in yeast strains with targeted deficiencies of genes important for ergosterol biosynthesis (that is, *erg2*, *erg3* and *erg6*)[29] by revealing a hypersensitivity to PUFA supplementation in cells unable to generate sterol with the characteristic unsaturated B-ring structure (Extended Data Fig. 6c,d).

To investigate the impact of 7-DHC in a well-defined phospholipid autoxidation model, we prepared unilamellar liposomes of soy phosphatidylcholine (PC) loaded with 7-DHC (Fig. 3a). We used the recently developed FENIX assay to indirectly monitor in real time the process of phospholipid peroxidation[30]. The assay relies on the specific generation of lipid peroxyl radicals arising from the lipophilic radical generator di-*tert*-undecylhyponitrite (DTUN). A small amount of STY-BODIPY dye competes with PUFA for propagating lipid peroxyl radicals and the fluorescence of its oxidized product(s), STY-$BODIPY_{ox}$, can be monitored by fluorescence (Fig. 3a). Typical radical-trapping antioxidants inhibit autoxidation and thus retard STY-BODIPY oxidation until the radical-trapping antioxidant is consumed (Fig. 3a,b). Interestingly, 7-DHC-loaded liposomes resulted in a dose-dependent suppression of STY-BODIPY oxidation (Fig. 3b,c). As the suppression of STY-BODIPY oxidation could arise from dilution of the pool of

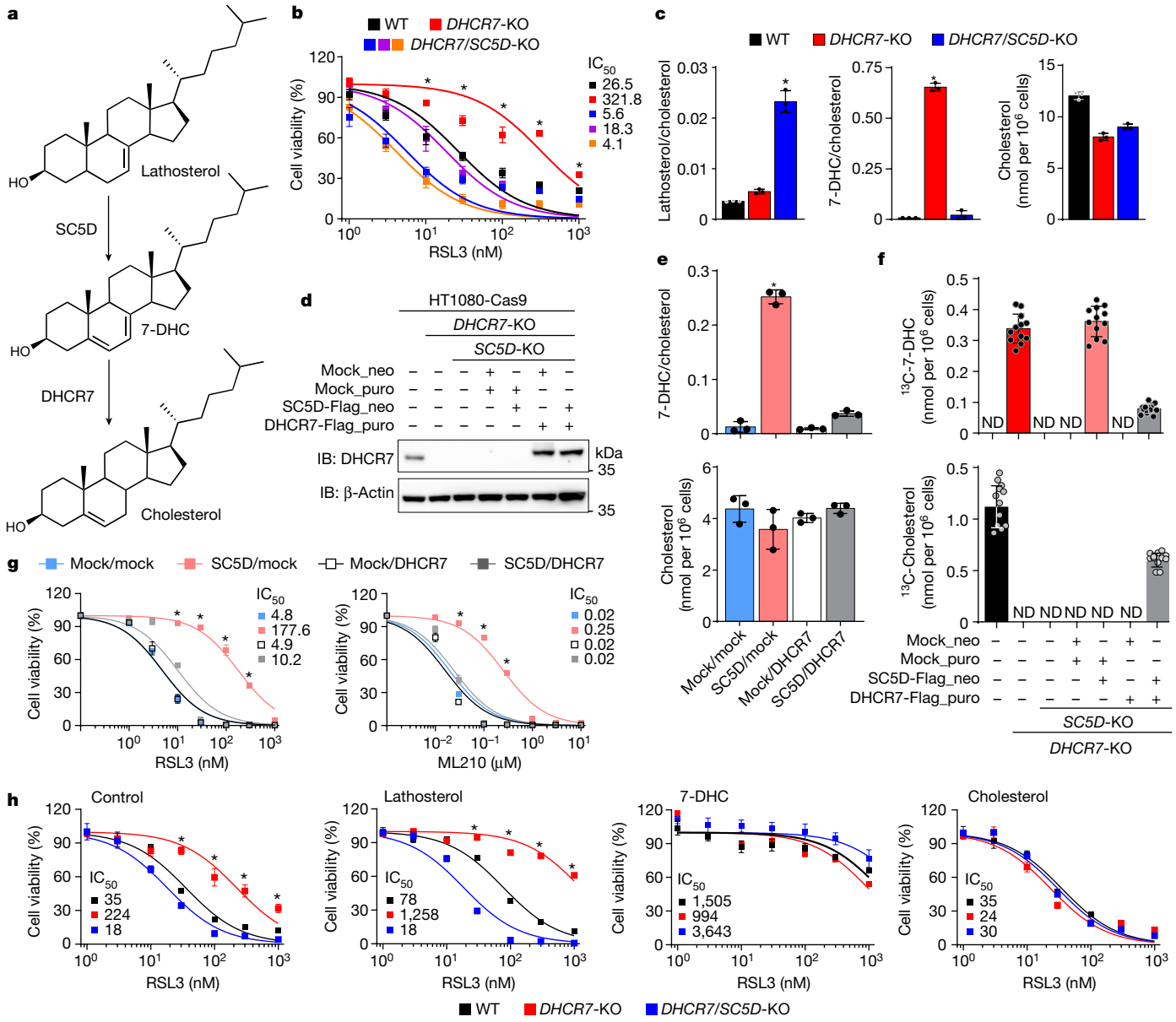

Fig. 2 | 7-DHC accumulation suppresses ferroptosis. a, Schematic of final steps of cholesterol biosynthesis. **b**, Dose-dependent toxicity of RSL3 in HT1080 Cas9 WT, *DHCR7* and *DHCR7 SC5D* KO cell lines. **c**, Relative quantification of lathosterol, 7-DHC and cholesterol concentrations in HT1080 Cas9 WT, *DHCR7* and *DHCR7 SC5D* KO cell lines. **d**, Immunoblotting for DHCR7 in HT1080 Cas9 expressing the indicated lentiviral constructs. β-ACTIN was used as a loading control. **e**, Relative quantification of 7-DHC and cholesterol concentrations in HT1080 Cas9 *DHCR7 SC5D* KO stably overexpressing SC5D and DHCR7 (SC5D/DHCR7), only SC5D (SC5D/mock), only DHCR7 (mock/DHCR7) and an empty vector (mock/mock). **f**, Assessment of de novo cholesterol biosynthesis, by means of the quantification of ^{13}C-cholesterol and ^{13}C-7-DHC originating from ^{13}C-glucose, in HT1080 Cas9 in the indicated genotypes. **g**, Dose-dependent toxicity of the ferroptosis inducers RSL3 and ML210 in the HT1080 cell lines described in **e**,**f**. **h**, Effect of sterol supplementation [10 μM] on RSL3 toxicity in HT1080 Cas9 WT, *DHCR7* and *DHCR7 SC5D* KO cell lines. Cell viability was assessed after 24 h (**b**) or 48 h using Alamar blue (**g**,**h**). Data are the mean ± s.d. of $n = 3$ wells of a 96-well plate (**b**,**g**,**h**) or a 6-well plate (**c**,**e**,**f**) from two (**b**,**h**) or three (**g**) or one (**c**,**f**) independent experiments. $^*P < 0.05$; two-way ANOVA (**b**,**c**,**e**,**g**,**h**).

autoxidizable phospholipids on supplementation of the liposomes with 7-DHC, similar experiments, wherein non-oxidizable dipalmitoyl PC (DPPC) was incorporated in place of 7-DHC, were performed, allowing us to demonstrate no difference from the native soy PC liposomes (Fig. 3b). Furthermore, because sterols alter membrane fluidity and may confer protection through dynamic parameters[31] that could impact lipid peroxidation[32], corresponding experiments were carried out on cholesterol-loaded liposomes (Fig. 3c). Yet again, there was no effect on the rate of STY-BODIPY oxidation—even beyond concentrations of 7-DHC used (Extended Data Fig. 7a)—suggesting that physical changes in the bilayer imparted by the sterol framework do not impact the oxidation rates in our model system, neither do they impact their integrity (Extended Data Fig. 7b). Given the indirect nature of the assay, we also directly measured the impact of 7-DHC on soy PC peroxidation, that is palmitoyl-linoleoyl PC (PLPC)-OOH, dilinoleoyl PC (DLPC)-OOH and DLPC-2OOH, by liquid chromatography with tandem mass spectrometry (LC–MS/MS) (Extended Data Fig. 7d,e). Although supplementation of the liposomes with DPPC (up to 32 mol%) had no effect on the rate of PLPC and DLPC oxidation, cholesterol (at 8 mol%) had only a modest effect on the accumulation of PLPC-OOH, DLPC-OOH and DLPC-2OOH. Entirely consistent with the FENIX results, 7-DHC supplementation led to a dose-dependent suppression in the rate of PLPC

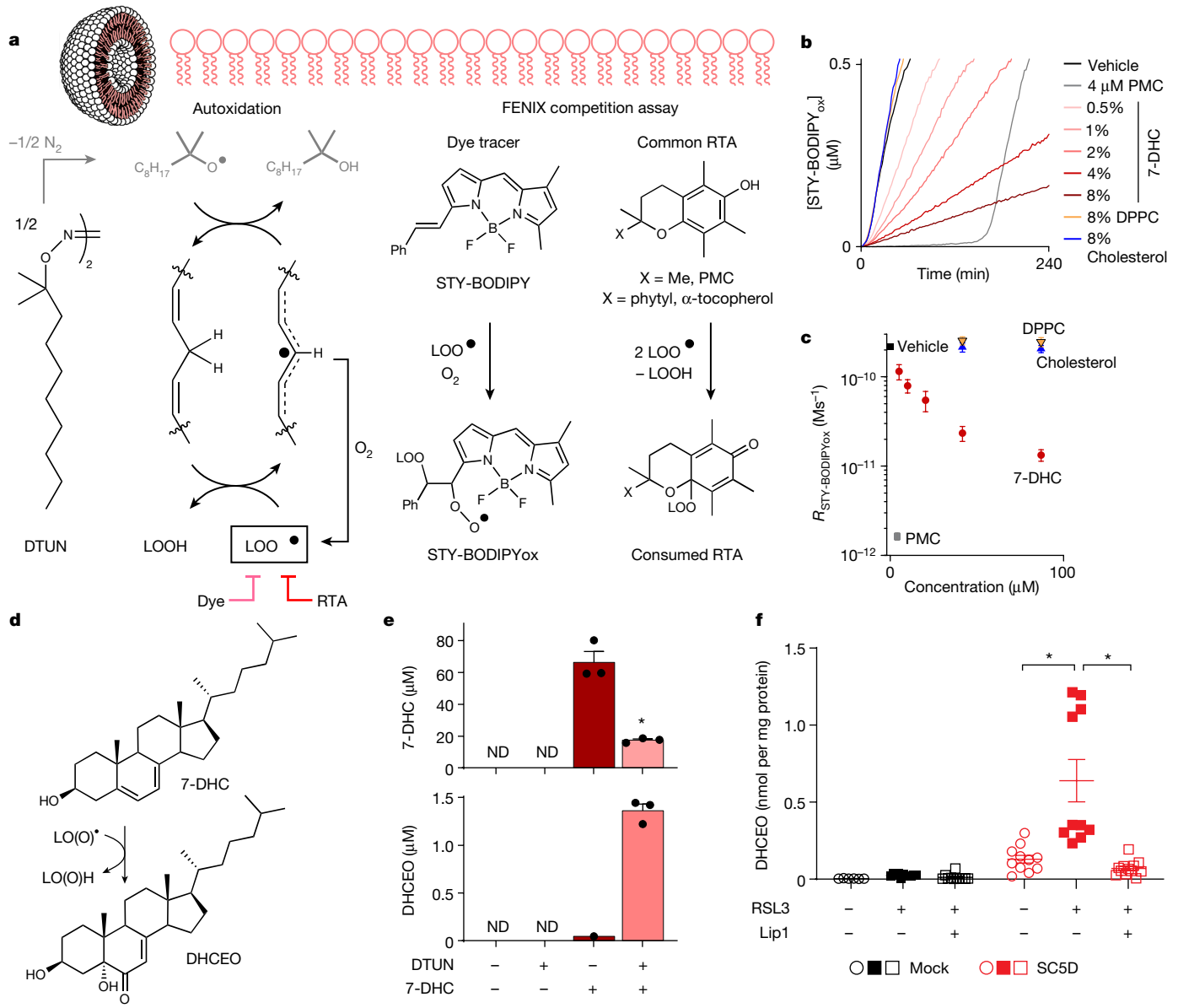

Fig. 3 | 7-DHC acts to suppress (phospho)lipid peroxidation. a, Liposomes of soy PC (1 mM) supplemented with cholesterol, 7-DHC or DPPC were prepared and autoxidized using DTUN [200 nM]. STY-BODIPY co-autoxidations are monitored by fluorescence of oxidized STY-BODIPY. PMC, 2,2,5,7,8-pentamethyl-6-chromanol. **b**, Representative data from co-autoxidations of STY-BODIPY [1 μM] and liposomal soy PC. **c**, The rates of STY-BODIPYox formation plotted as a function of additive concentration. **d**, Schematic of 7-DHC oxidation highlighting DHCEO as the main detectable oxidation products. **e**, Quantification of 7-DHC and DHCEO in liposome with and without 7-DHC in the absence or presence of DTUN for 2 h. **f**, Quantification of DHCEO in HT1080 *SC5D DHCR7* double-KO cells expressing empty vector (black) and SC5D (red) on [200 nM] RSL3 with and without 500 nM Lip1 for 6 h. Data are the representative of one independent experiment (**b**,**c**) or the mean ± s.d. of $n = 3$ technical replicates of a 6 cm plate from two independent experiments (**e**,**f**). *$P < 0.05$; two-way ANOVA (**e**,**f**).

and DLPC oxidation (Extended Data Fig. 7d,e) which is in good agreement with previous reports in isotropic media[33]. To demonstrate that this suppression corresponded with the intervention of 7-DHC in the radical chain reaction, the consumption of 7-DHC was monitored spectrophotometrically through its characteristic absorbance (Extended Data Fig. 7f,g). These data thus suggest that the oxidation of 7-DHC in vitro is responsible for the inhibition of phospholipid peroxidation, a notion we could further validate in a model using iron/ascorbate as the source of oxidation (Extended Data Fig. 7h). Accordingly, we detected significant concentrations of the free radical-mediated oxidation product of 7-DHC, namely 3β,5α-dihydroxycholest-7-en-6-one (DHCEO) (Fig. 3d), during the liposomal oxidation under conditions where no phospholipid oxidation product was detectable (Fig. 3e). Hence, if our hypothesis was correct, 7-DHC oxidation should lead to the accumulation of these products during the course of ferroptosis and by doing so, it could spare phospholipids from oxidative damage. To assess whether 7-DHC oxidation products also accumulate on triggering ferroptosis in cells, we treated the HT1080 *DHCR7 SC5D* double-KO cell line expressing SC5D and an empty vector with the GPX4 inhibitor RSL3. Although no substantial loss in the total content of 7-DHC was noticeable (Extended Data Fig. 7i), the quantification of the main non-enzymatic oxidation products of 7-DHC, namely DHCEO, revealed a significant increase (Fig. 3f and Extended Data Fig. 7i). To demonstrate that the 7-DHC products originate from the peroxyl radical-mediated oxidation of 7-DHC, we further incubated these cells with Lip1 (ref. 9). In good agreement with the free radical-mediated formation of DHCEO[25], Lip1 fully inhibited the formation of this product (Fig. 3f and Extended Data Fig. 7i). Therefore, these results firmly establish a unique role of

unsaturated B-ring sterols in protecting cells from ferroptosis-like cell death by diverting the propagation of peroxyl radical-mediated damage from phospholipid components to its sterol core.

Truncated phospholipids drive cell lysis

Following these results, we reasoned that the presence of 7-DHC in phospholipid bilayers generates a strong prosurvival effect by increasing the resistance of membranes to peroxidation-mediated permeabilization. Therefore, a model system was used that consists of 5(6)-carboxyfluorescein (CF) encapsulated in liposomes allowing for the detection of a fluorescent signal on membrane permeabilization (Extended Data Fig. 8a). Using the iron/ascorbate couple as an oxidation model, we showed that liposomes containing 7-DHC were markedly resistant to peroxidation-mediated membrane permeabilization (Extended Data Fig. 8b). To further support the relevance of this model system for ferroptosis, we could show that the process of vesicle rupture could be prevented by Lip1 (Extended Data Fig. 8c) and other molecules able to suppress ferroptosis, such as ergosterol, ubiquinone, α-tocopherol and squalene (Extended Data Fig. 8d), indicating that Lip1 and naturally occurring ferroptosis supressors could act similarly to prevent membrane permeabilization of cells.

Recent reports studying the relative contribution of different photosensitization mechanisms to membrane permeabilization suggested that truncated phospholipid species rather than phospholipid hydroperoxides are key in generating membrane pores and consequently mediating the loss of membrane integrity[34]. Therefore, we reasoned that a similar mechanism could be at play during iron-induced permeabilization and ferroptosis execution[35]. To establish a functional link between truncated lipids and ferroptosis execution, we initially assayed a panel of different truncated species (Extended Data Fig. 9a) regarding their capacity to destabilize membranes. Accordingly, all tested truncated lipids were able to permeabilize liposomal membranes and to induce cell death more efficiently than the parental lipid and the corresponding hydroperoxide (Extended Data Fig. 9b–e). Further validation was provided by using an orthogonal approach based on a photochemical probe (PhotoPC). Irradiation of the probe directly generates a truncated product (PhotoTrunc-PC) which does not rely on the presence of alkoxyl or peroxyl radicals intermediate (Extended Data Fig. 9f). Using this model we could demonstrate the higher membrane destabilizing capacity of the truncated product in vesicles and cells (Extended Data Fig. 9g,h). Although being highly supportive, it should be acknowledged that the truncated species were added exogenously and were performed using PC and not PE species[12,14]. To circumvent this issue, a system in which the species are formed in situ would be preferred. We took advantage of the cell's own fatty acid incorporation machinery to achieve this goal. ACSL4-deficient cells have a profound loss of PUFA content in phospholipids[12]. The absence of PUFA containing phospholipids results in a marked resistance to ferroptosis because of the lack of oxidizable substrates. Sensitivity to ferroptosis in this setting can be regained by feeding exogenous PUFAs[12]. This feature can be leveraged to better control of the substrates used for ferroptosis execution. Using this model, we compared side-by-side the sensitization provided by α-linolenic acid (αLNN) and γ-linolenic acid (γLNN). Both fatty acids have an identical structure in length and number of double bonds leading to a similar propagation rate constant (k_p), yet the position of the last double-bond determines the structure of the resulting truncated product. Analysis of the lipidomic changes of *ACSL4* WT and KO cells treated with αLNN and γLNN confirmed that both lipids are directly and efficiently esterified into PE, thereby restoring the oxidizable pool of PUFA to a similar extent as in WT cells (Extended Data Fig. 10a,b). Remarkably, despite their equal abundance and propensity to undergo oxidation, γLNN seemed to be a superior ferroptosis-triggering substrate (Extended Data Fig. 10c,d), in line with its potential to generate shorter truncated phospholipid products. These results are remarkable because they indicate that the product formed determines cell death rather than solely its propensity to autoxidize. Supporting this notion, in-depth epilipidomics analysis indeed detected a substantial accumulation of PE and plasmalogen PE truncated products in cells undergoing ferroptosis (Fig. 4a). Notably, cell permeabilization, monitored as propidium iodide (PI)-positive cells, was only detectable in conditions where an increase in these oxidized and truncated species occurred (Fig. 4b). We further showed that Lip1 fully inhibited the formation of these species, thus confirming their origin from the autocatalytic lipid peroxidation process (Fig. 4a,b). In accordance, cells accumulating 7-DHC behaved similarly to Lip1-treated cells and the specific oxidation product of 7-DHC, DHCEO, accumulated in these cells (Fig. 4b). This demonstrates that 7-DHC is preferentially oxidized in cells, thereby sparing phospholipids and preventing the formation of oxidized and truncated species (Extended Data Fig. 9i). Supporting the proposed mechanism, 7-DHC did not affect permeabilization mediated by truncated phospholipid species (Extended Data Fig. 9e). Together, these observations provide compelling evidence for the role of truncated products in contributing to ferroptosis execution and that 7-DHC and other ferroptosis inhibitors such as Lip1, directly suppress their formation.

7-DHC accumulation increases cell fitness

Having characterized the molecular underpinnings by which 7-DHC prevents ferroptosis execution, we next asked whether this protective effect could have a potential role in supporting tumour growth under conditions in which ferroptosis inhibition is critical. To our initial surprise, *DHCR7* mutations, despite being rare, have been described in people with Burkitt's lymphoma (BL), with a reported 9.8% frequency of DHCR7 mutations as shown by ref. 36. Moreover, a recent report has also identified rare pathological mutations in DHCR7 in a cohort with neuroblastoma[37]. To gain insights into the topology of these mutations, we created a model for the DHCR7 structure using an homologous structure (PDB ID 4QUV, sequence identity 37%, similarity 51%) and identified that they are primarily located in the transmembrane domain of DHCR7 (Fig. 5a). Re-expression of *DHCR7*-Flag-tagged versions of the seven corresponding mutants in the *DHCR7*-deficient cells allowed us to validate these predictions experimentally. Figure 5b illustrates that, except for T93M, N274K and V353fs, all mutations were generally well expressed as compared to WT. We then addressed the functionality of these mutations: the A24S and L317V mutations seemed to be functional when overexpressed as they were able to (1) metabolize 7-DHC when overexpressed (Fig. 5c) and (2) to re-sensitize *DHCR7*-deficient cells to ferroptosis akin to the WT enzyme (Fig. 5d). On the other hand, all other assayed variants were dysfunctional and failed to metabolize 7-DHC (Fig. 5c) and were unable to restore sensitivity to ferroptosis (Fig. 5d). Further validation of the role of the DHCR7 was pursued by demonstrating that 7-DHC accumulation abolished the characteristic thiol-dependent growth of Burkitt's lymphoma cell lines in the absence of thiol-donating compound (Extended Data Fig. 11a,b).

Next, the contribution of 7-DHC accumulation and tumour growth in a series of xenograft models was investigated. Initially, we deleted DHCR7 in two different cell lines: BL41 (a Burkitt's lymphoma cell line) and MM1S (a multiple myeloma cell line). These cell lines showed distinct responses to ferroptosis when DHCR7 is deleted; whereas BL41 cells showed a significant increase in resistance against GPX4 inhibitors (Fig. 5e), the protective effect in MM1S cells was negligible (Extended Data Fig. 12a,b). Accordingly, when implanted into the tail vein of mice, the MM1S xenograft did not show any noticeable behavioural differences, in line with the absence of extra protective effect caused by DHCR7 loss (Extended Data Fig. 12c,d). By marked contrast, the DHCR7-deficient BL41 cell line showed a significantly more aggressive phenotype compared to its WT counterpart with marked decrease in overall survival of mice (±24 days versus ±60 days) (Fig. 5f–i).

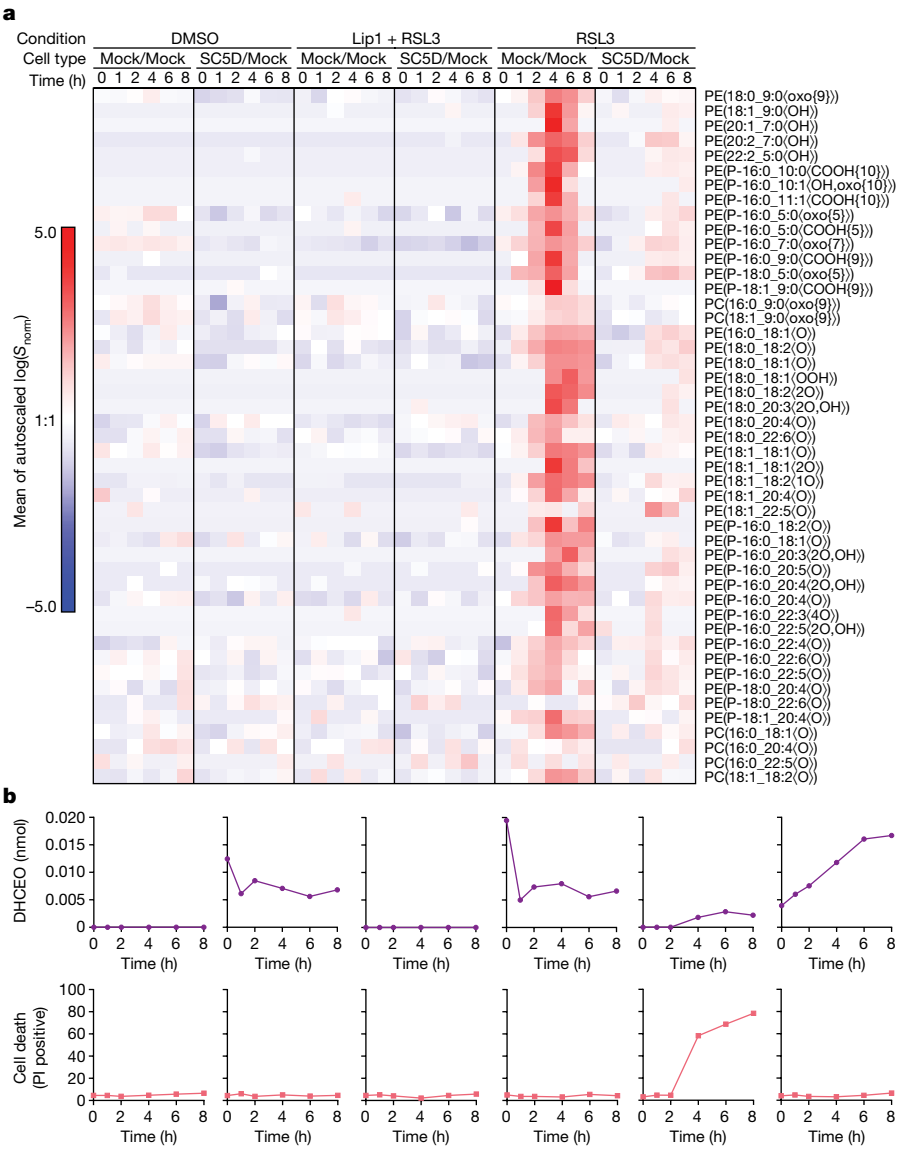

Fig. 4 | Phospholipid truncated species contribute to ferroptosis execution. **a**, Epilipidomics analysis of HT1080 Cas9 *DHCR7 SC5D* double-KO cells overexpressing SC5D or an empty vector. Data are representative of one experiment performed five times independently (results from the other repetitions are in the Supplementary Information). **b**, Cell death (PI positive) and DHCEO values from matched experimental time points of samples depicted in **a**.

To further substantiate whether this effect was attributed to increased resistance to ferroptosis, we performed an independent experiment where the growth of BL41 xenografts was compared in mice maintained on a selenium-adequate and -deprived diet (Extended Data Fig. 12e–h). This model mimics an in vivo 'ferroptosis-prone' condition[38] by limiting the supply of selenium for the translation of selenoproteins, including GPX4 (Extended Data Fig. 12f). Under this proferroptotic conditions, an even more pronounced difference in tumour growth was observed (Extended Data Fig. 12g), strengthening the notion that ferroptosis-sensitive cancer cell lines benefit from the accumulation of 7-DHC and that its accumulation favours tumour growth by suppressing ferroptosis. In addition to this model, we also used an orthotopic neuroblastoma model (Extended Data Fig. 12i–p) using the ferroptosis-sensitive neuroblastoma cell line SK-N-DZ. Deletion of DHCR7 in SK-N-DZ cells provided a robust protection against GPX4 inhibitors (Extended Data Fig. 12i–l). Orthotopic implantation of these cells in the adrenal gland of mice led to a more aggressive phenotype, as indicated by the reduced survival of mice implanted with DHCR7-deficient cells (Extended Data Fig. 12m,n). Interestingly, and in agreement with the reduced survival, analysis of these mice showed a massive increase in the incidence of lung metastasis in the DHCR7-deficient neuroblastoma group (Extended Data Fig. 12o,p); we speculate that ferroptosis-sensitive tumour cell lines, such as SK-N-DZ and BL41, benefit from mechanisms that protect against ferroptosis in the bloodstream[39]. Collectively, our data indicate that in ferroptosis-sensitive cell lines, the extra survival advantage conferred by accumulating 7-DHC promotes a more aggressive phenotype in vivo.

Discussion

Our work introduces and characterizes an unforeseen role for DHCR7 in modulating ferroptosis. Although many reverse and forward genetic screens have been performed to identify regulators of ferroptosis, DHCR7 has not consistently emerged as a regulator—unlike ACSL4, for example[13,40]. Possible factors affecting DHCR7 inhibition and 7-DHC accumulation include defects in the cholesterol biosynthesis pathway and the impact of free cholesterol on the mevalonate pathway, a notion supported by our results. We now provide a comprehensive

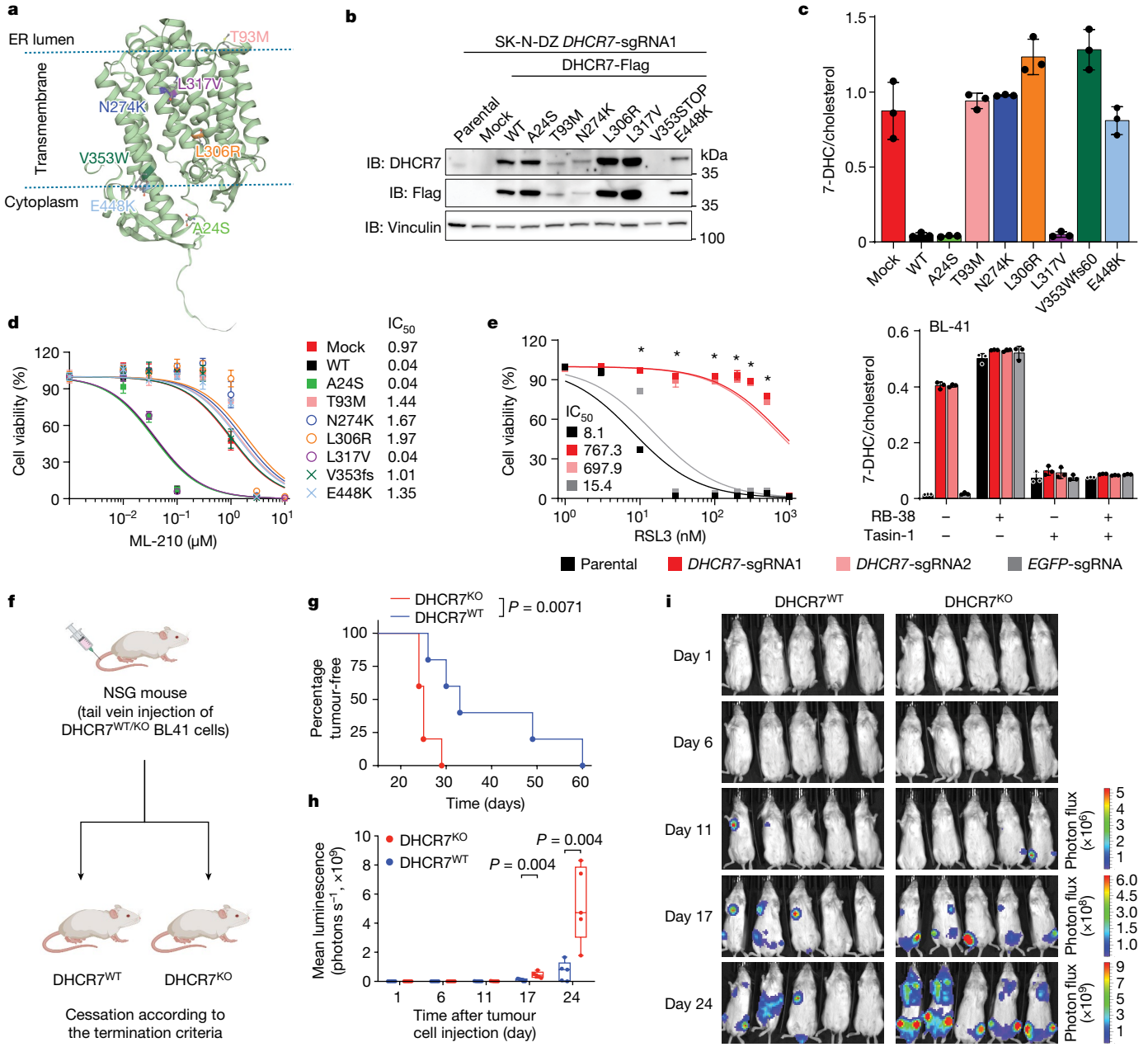

Fig. 5 | Impact of 7-DHC accumulation on lymphoma growth. a, Homology model of the DHCR7 structure based on the sterol reductase from *M. alcaliphilum*. Mutations are indicated as ball and stick. **b**, Immunoblot analysis of the levels of expression of DHCR7, FLAG-tagged DHCR7 WT and mutant versions reported in patients with Burkitt's lymphoma or neuroblastoma in a SK-N-DZ-*DHCR7* KO cell line. **c**, Relative quantification of 7-DHC in a SK-N-DZ-*DHCR7* KO cell line expressing FLAG-tagged *DHCR7* WT and the indicated mutants. Data are the mean ± s.d. of triplicates from a 6-well plate from one representative experiment. **d**, Dose-dependent toxicity of the ferroptosis inducer ML210 in SK-N-DZ expressing FLAG-tagged *DHCR7* WT and the indicated mutants. **e**, Left, dose-dependent toxicity of RSL3 in BL41 expressing two independent sgRNA targeting *DHCR7* and *EGFP*. Right, relative quantification of 7-DHC concentrations in the BL41 cell line treated with RB38 and Tasin-1. Cell viability was assessed after 48 h using Alamar blue; data are the mean ± s.d. of $n = 3$ wells of a 96-well plate (**d**,**e**) from two (**d**) or three (**e**) independent experiments. $^*P < 0.05$; two-way ANOVA (**e**). **f**, Schematic representation of the tail vein injection of control ($DHCR7^{WT}$) or DHCR7-deficient ($DHCR7^{KO}$) BL41 cell line. **g**, Kaplan–Meier plot displaying tumour-free survival for mice injected with $DHCR7^{WT}$ (blue, $n = 5$) or $DHCR7^{KO}$ (red, $n = 5$) BL41 cells, a log-rank (Mantel–Cox) test was conducted for statistical analysis; *P* value indicated. **h**, Tumour growth on implantation of $DHCR7^{WT}$ (blue, $n = 5$) or $DHCR7^{KO}$ (red, $n = 5$) of BL41 cell line. Data represent the mean ± s.e.m.; Mann–Whitney test one-tailed, *P* values are indicated. In each box, horizontal lines denote mean values, whereas the box contains the 25th to 75th percentiles of dataset and whiskers mark the 5th and 95th percentiles. **i**, Representative luminescence images from each group are shown (**g**,**h**). Images in **f** created with BioRender.com.

understanding of the protective role of B-ring-unsaturated sterols against phospholipid peroxidation and ferroptosis. Using 7-DHC and ergosterol as two representatives of this class of sterols, we show that the specific and robust protection against phospholipid peroxidation is a feature that is not limited to only mammalian cells but is shared between biologically distant organisms.

This discovery in itself poses a paradox: a lipid frequently reported to propagate radical chain reaction[25,41] is capable of suppressing a cell death modality known to exclusively depend on these same biochemical events[15,42]. Initial studies have firmly established that, in cells undergoing ferroptosis, phospholipids furnished with PUFAs are the prime target for oxidation[14]. We now expand on this concept as we provide ample

evidence supporting their role in ferroptosis execution through the formation of membrane destabilizing truncated phospholipid species. These observations thus imply that lipid peroxidation can be uncoupled from cell death as only products of phospholipid peroxidation generate efficient ferroptosis-inducing metabolites. By having established this interrelationship, these seemingly paradoxical findings can now be rationalized. Molecules able to suppress the peroxidation of fatty acids esterified into phospholipid species need to efficiently outcompete PUFAs during lipid peroxidation and stabilize radical chain propagating species. Mechanistically, in isotropic solution, PUFAs have reported propagation rate constants (k_p) ranging from 62 in linoleic acid up to 197 M^{-1} s^{-1} for arachidonic acid, both of which can be easily outcompeted by 7-DHC given its extremely high (k_p) of 2,260 M^{-1} s^{-1}. This renders 7-DHC a superior phospholipid shield when compared to other sterols (cholesterol (k_p) = 11 and lathosterol (k_p) = 57 M^{-1} s^{-1}). Despite 7-DHC and other B-ring-unsaturated sterols being principal contributors and targets of lipid peroxidation, radicals derived from these sterol metabolites are poor inducers of cell death, unlike radicals in phospholipids that can give rise to membrane-destabilizing truncated species.

Together with the accompanying paper[20], we demonstrate that this process can be exploited to suppress ferroptosis in different settings. Specifically, inspired by the report that rare mutations in DHCR7 have been reported in both patients with Burkitt's lymphoma and patients with neuroblastoma, we demonstrate that the accumulation of 7-DHC can lead to a more aggressive phenotype in xenograft models relevant to both entities, thus presenting a potential compensatory mechanism for their intrinsic sensitivity to ferroptosis. This recognition could be relevant as recent reports have indicated that amplification of *MYC* and *MYCN* increase sensitivity to ferroptosis[43–46] and extra mechanism preventing ferroptosis in these oncogenic contexts could enhance cancer cell fitness. The ferroptosis-modulating activity of 7-DHC raises another noteworthy aspect; several recent screening studies have identified a series of FDA-approved drugs able to inhibit DHCR7 at nM concentrations[47]. For example, trazodone is prescribed more than 20 million times a year in the USA, sometimes off-label as a sleep aid; studies of patients on this drug have reported increased plasma concentrations of 7-DHC[48]. Epidemiological studies will be required to explore whether there are any groups of patients who regularly consume ferroptosis-modulating drugs and whether this has any impact on cancer incidence, metastasis occurrence or other public health-relevant aspects.

Interestingly, some organisms seem to have shifted away from this strategy. Specifically, DHCR7-like enzymes convert *5,7*-unsaturated sterols to the less autoxidizable sterols, such as cholesterol, thus keeping the concentration of B-ring unsaturated sterols low. The replacement of 7-DHC with cholesterol in humans offers clear benefits; this is documented by the causative role of DHCR7 mutations and the developmental syndrome known as Smith–Lemli–Opitz syndrome. This syndrome is characterized by varying levels of neurodevelopmental defects depending on the severity of the mutation. However, our findings reveal a paradoxical aspect. Whereas previous studies have shown that oxidation products of 7-DHC are toxic to neuronal cells[3] and can suppress key (neuro)developmental pathways like the Wnt/β-catenin[49] and Hedgehog[50] signal pathways, our study presents a contrasting perspective. We have observed the accumulation of 7-DHC oxidation formed during the process of preventing phospholipid peroxidation in cancer cells exposed to oxidants, such as conditions that induce ferroptosis. These findings emphasize the complex and context-dependent nature of 7-DHC and its oxidation products in different cellular contexts.

Ultimately, the mechanisms described here shed light in an unrecognized and primitive tolerance mechanism toward phospholipid peroxidation that could be highjacked by cancer cells to evade ferroptosis.

Online content

Any methods, additional references, Nature Portfolio reporting summaries, source data, extended data, supplementary information, acknowledgements, peer review information; details of author contributions and competing interests; and statements of data and code availability are available at https://doi.org/10.1038/s41586-023-06878-9.

1. Stockwell, B. R. Ferroptosis turns 10: emerging mechanisms, physiological functions and therapeutic applications. *Cell* **185**, 2401–2421 (2022).
2. Dos Santos, A. F., Fazeli, G., Xavier da Silva, T. N. & Friedmann Angeli, J. P. Ferroptosis: mechanisms and implications for cancer development and therapy response. *Trends Cell Biol.* **33**, 1062–1076 (2023).
3. Korade, Z., Xu, L., Shelton, R. & Porter, N. A. Biological activities of 7-dehydrocholesterol-derived oxysterols: implications for Smith–Lemli–Opitz syndrome. *J. Lipid Res.* **51**, 3259–3269 (2010).
4. Yin, H., Xu, L. & Porter, N. A. Free radical lipid peroxidation: mechanisms and analysis. *Chem. Rev.* **111**, 5944–5972 (2011).
5. Angeli, J. P. F., Shah, R., Pratt, D. A. & Conrad, M. Ferroptosis inhibition: mechanisms and opportunities. *Trends Pharmacol. Sci.* **38**, 489–498 (2017).
6. Seiler, A. et al. Glutathione peroxidase 4 senses and translates oxidative stress into 12/15-lipoxygenase dependent- and AIF-mediated cell death. *Cell Metab.* **8**, 237–248 (2008).
7. Yant, L. J. et al. The selenoprotein GPX4 is essential for mouse development and protects from radiation and oxidative damage insults. *Free Radic. Biol. Med.* **34**, 496–502 (2003).
8. Yang, W. S. et al. Regulation of ferroptotic cancer cell death by GPX4. *Cell* **156**, 317–331 (2014).
9. Friedmann Angeli, J. P. et al. Inactivation of the ferroptosis regulator Gpx4 triggers acute renal failure in mice. *Nat. Cell Biol.* **16**, 1180–1191 (2014).
10. Ursini, F., Maiorino, M., Valente, M., Ferri, L. & Gregolin, C. Purification from pig liver of a protein which protects liposomes and biomembranes from peroxidative degradation and exhibits glutathione peroxidase activity on phosphatidylcholine hydroperoxides. *Biochim. Biophys. Acta* **710**, 197–211 (1982).
11. Nishida Xavier da Silva, T., Friedmann Angeli, J. P. & Ingold, I. GPX4: old lessons, new features. *Biochem. Soc. Trans.* **50**, 1205–1213 (2022).
12. Doll, S. et al. ACSL4 dictates ferroptosis sensitivity by shaping cellular lipid composition. *Nat. Chem. Biol.* **13**, 91–98 (2017).
13. Zou, Y. et al. A GPX4-dependent cancer cell state underlies the clear-cell morphology and confers sensitivity to ferroptosis. *Nat. Commun.* **10**, 1617 (2019).
14. Kagan, V. E. et al. Oxidized arachidonic and adrenic PEs navigate cells to ferroptosis. *Nat. Chem. Biol.* **13**, 81–90 (2017).
15. Shah, R., Shchepinov, M. S. & Pratt, D. A. Resolving the role of lipoxygenases in the initiation and execution of ferroptosis. *ACS Cent. Sci.* **4**, 387–396 (2018).
16. Pedrera, L. et al. Ferroptotic pores induce Ca(2+) fluxes and ESCRT-III activation to modulate cell death kinetics. *Cell Death Differ.* **28**, 1644–1657 (2021).
17. Riegman, M. et al. Ferroptosis occurs through an osmotic mechanism and propagates independently of cell rupture. *Nat. Cell Biol.* **22**, 1042–1048 (2020).
18. Kandutsch, A. A. & Russell, A. E. Preputial gland tumor sterols. 3. A metabolic pathway from lanosterol to cholesterol. *J. Biol. Chem.* **235**, 2256–2261 (1960).
19. Xu, L., Davis, T. A. & Porter, N. A. Rate constants for peroxidation of polyunsaturated fatty acids and sterols in solution and in liposomes. *J. Am. Chem. Soc.* **131**, 13037–13044 (2009).
20. Li, Y. et al. 7-Dehydrocholesterol dictates ferroptosis sensitivity. *Nature*, https://doi.org/10.1038/s41586-023-06983-9 (2024).
21. Tzelepis, K. et al. A CRISPR dropout screen identifies genetic vulnerabilities and therapeutic targets in acute myeloid leukemia. *Cell Rep.* **17**, 1193–1205 (2016).
22. Yuan, H., Li, X., Zhang, X., Kang, R. & Tang, D. Identification of ACSL4 as a biomarker and contributor of ferroptosis. *Biochem. Biophys. Res. Commun.* **478**, 1338–1343 (2016).
23. Dixon, S. J. et al. Human haploid cell genetics reveals roles for lipid metabolism genes in nonapoptotic cell death. *ACS Chem. Biol.* **10**, 1604–1609 (2015).
24. Zou, Y. et al. Plasticity of ether lipids promotes ferroptosis susceptibility and evasion. *Nature* **585**, 603–608 (2020).
25. Xu, L., Korade, Z. & Porter, N. A. Oxysterols from free radical chain oxidation of 7-dehydrocholesterol: product and mechanistic studies. *J. Am. Chem. Soc.* **132**, 2222–2232 (2010).
26. Conrad, M. & Pratt, D. A. The chemical basis of ferroptosis. *Nat. Chem. Biol.* **15**, 1137–1147 (2019).
27. Garcia-Bermudez, J. et al. Squalene accumulation in cholesterol auxotrophic lymphomas prevents oxidative cell death. *Nature* **567**, 118–122 (2019).
28. Westover, E. J. & Covey, D. F. The enantiomer of cholesterol. *J. Membr. Biol.* **202**, 61–72 (2004).
29. Johnston, E. J., Moses, T. & Rosser, S. J. The wide-ranging phenotypes of ergosterol biosynthesis mutants and implications for microbial cell factories. *Yeast* **37**, 27–44 (2020).
30. Shah, R., Farmer, L. A., Zilka, O., Van Kessel, A. T. M. & Pratt, D. A. Beyond DPPH: use of fluorescence-enabled inhibited autoxidation to predict oxidative cell death rescue. *Cell Chem. Biol.* **26**, 1594–1607 (2019).
31. Zhang, X., Barraza, K. M. & Beauchamp, J. L. Cholesterol provides nonsacrificial protection of membrane lipids from chemical damage at air–water interface. *Proc. Natl Acad. Sci. USA* **115**, 3255–3260 (2018).
32. McLean, L. R. & Hagaman, K. A. Effect of lipid physical state on the rate of peroxidation of liposomes. *Free Radic. Biol. Med.* **12**, 113–119 (1992).
33. Do, Q. et al. Development and application of a peroxyl radical clock approach for measuring both hydrogen-atom transfer and peroxyl radical addition rate constants. *J. Org. Chem.* **86**, 153–168 (2021).
34. Bacellar, I. O. L. et al. Photosensitized membrane permeabilization requires contact-dependent reactions between photosensitizer and lipids. *J. Am. Chem. Soc.* **140**, 9606–9615 (2018).
35. Friedmann-Angeli, J. P., Miyamoto, S. & Schulze, A. Ferroptosis: the greasy side of cell death. *Chem. Res. Toxicol.* **32**, 362–369 (2019).

36. Schmitz, R. et al. Burkitt lymphoma pathogenesis and therapeutic targets from structural and functional genomics. *Nature* **490**, 116–120 (2012).
37. Bonfiglio, F. et al. Inherited rare variants in homologous recombination and neurodevelopmental genes are associated with increased risk of neuroblastoma. *EBioMedicine* **87**, 104395 (2023).
38. Eagle, K. et al. An oncogenic enhancer encodes selective selenium dependency in AML. *Cell Stem Cell* **29**, 386–399 (2022).
39. Ubellacker, J. M. et al. Lymph protects metastasizing melanoma cells from ferroptosis. *Nature* **585**, 113–118 (2020).
40. Zou, Y. et al. A GPX4-dependent cancer cell state underlies the clear-cell morphology and confers sensitivity to ferroptosis. *Nat. Commun.* **10**, 1617 (2019).
41. Xu, L. & Porter, N. A. Reactivities and products of free radical oxidation of cholestadienols. *J. Am. Chem. Soc.* **136**, 5443–5450 (2014).
42. Zilka, O. et al. On the mechanism of cytoprotection by ferrostatin-1 and liproxstatin-1 and the role of lipid peroxidation in ferroptotic cell death. *ACS Cent. Sci.* **3**, 232–243 (2017).
43. Lu, Y. et al. MYCN mediates TFRC-dependent ferroptosis and reveals vulnerabilities in neuroblastoma. *Cell Death Dis.* **12**, 511 (2021).
44. Floros, K. V. et al. MYCN-amplified neuroblastoma is addicted to iron and vulnerable to inhibition of the system Xc-/glutathione axis. *Cancer Res.* **81**, 1896–1908 (2021).
45. Alborzinia, H. et al. MYCN mediates cysteine addiction and sensitizes neuroblastoma to ferroptosis. *Nat. Cancer* **3**, 471–485 (2022).
46. Alborzinia, H. et al. LRP8-mediated selenocysteine uptake is a targetable vulnerability in MYCN-amplified neuroblastoma. *EMBO Mol. Med.* **15**, e18014 (2023).
47. Kim, H. Y. et al. Inhibitors of 7-dehydrocholesterol reductase: screening of a collection of pharmacologically active compounds in Neuro2a cells. *Chem. Res. Toxicol.* **29**, 892–900 (2016).
48. Hall, P. et al. Aripiprazole and trazodone cause elevations of 7-dehydrocholesterol in the absence of Smith–Lemli–Opitz syndrome. *Mol. Genet. Metab.* **110**, 176–178 (2013).
49. Francis, K. R. et al. Modeling Smith–Lemli–Opitz syndrome with induced pluripotent stem cells reveals a causal role for Wnt/beta-catenin defects in neuronal cholesterol synthesis phenotypes. *Nat. Med.* **22**, 388–396 (2016).
50. Sever, N. et al. Endogenous B-ring oxysterols inhibit the Hedgehog component Smoothened in a manner distinct from cyclopamine or side-chain oxysterols. *Proc. Natl Acad. Sci. USA* **113**, 5904–5909 (2016).

Reporting summary

Further information on research design is available in the Nature Portfolio Reporting Summary linked to this article.

Data availability

All data and materials to draw the conclusions in this paper are presented in the main text, figures and the extended data figures. Raw data from the (epi)lipidomics experiments are available at the repository MASSIVE (https://doi.org/10.25345/C5F47H47Z). Further data can be received from the corresponding author on reasonable request. CRISPR analysis and uncropped blot are presented in the Supplementary Information. Source data are provided with this paper.

Acknowledgements J.P.F.A. acknowledges the support of the Junior Group Leader programme of the Rudolf Virchow Center, University of Würzburg, the Deutsche Forschungsgemeinschaft (DFG) WE 5719/2-1, FR 3746/3-1, FR 3746/5-1 and FR 3746/6-1. J.P.F.A, I.W. and M.K. acknowledge the DFG CRC205 (INST 269/886-1). J.P.F.A. and R.C.B. are grateful for the support provided by the Interdisziplinäres Zentrum für klinische Forschung (IZKF, B-424) and the Deutsche Jose Carreras Leukämie Stiftung (DJCLS 01R/2022). R.C.B. acknowledges the DFG through grant BA 1596/7-1. A.T. acknowledges the DKTK joint funding project 'RiskY-AML'; the 'Integrate-TN' Consortium funded by the Deutsche Krebshilfe, the Dietmar Hopp Foundation and the European Research Council (ERC; AdG-101055270). M.F. receives financial support from the German Federal Ministry of Education and Research (BMBF) in the framework of the e:Med research and funding concept for SysMedOS project and FERROPath (01EJ2205A), 'Sonderzuweisung zur Unterstützung profilbestimmender Struktureinheiten 2021' by the SMWK, TG70 by Sächsische Aufbaubank and SMWK, the measure is co-financed with tax funds on the basis of the budget passed by the Saxon state parliament, Deutsche Forschungsgemeinschaft (FE 1236/5-1); further thanks goes to R. Hoffmann (Institute of Bioanalytical Chemistry, University of Leipzig) for providing access to his laboratory. M.C. acknowledges support from the DFG CO 291/7-1, the DFG SPP 2306 (CO 291/9-1, CO 291/10-1), BMBF VIP+ program NEUROPROTEKT (03VP04260) and the ERC (grant no. GA 884754). D.B.K. is grateful to the Fonds of the Chemical Industry for a Liebig fellowship. D.A.P. would like to thank the Natural Sciences and Engineering Council of Canada and the Canada Foundation for Innovation for their support. S.M. and A.I. acknowledge support from the São Paulo Research Foundation (FAPESP) 2013/07937-8 (CEPID Redoxoma) and 2017/13804-1. T.C.G.-M. and K.M. received support from the National Institutes of Health NIMH R01 MH110636. J.K.S. acknowledges National Science Foundation grants HDR: DIRSE-IL 1940169 and RAPID 2031614. D.F.C. acknowledges the NIH through grant P50 MH122379 and R01 HL067773. Further support through the DFG priority program SPP 2306 is acknowledged by M.F., M.C., D.B.K., A.G.J.S., A.T. and J.P.F.A. We are grateful to excellent technical assistance of T. Henninger, Z. Donova and A. Haberberger.

Author contributions F.P.F. carried out most of the in vitro experiments with contributions from H.N., A.F.S., T.N.X.S., S.A., Z.C. S.M., and A.I. S.M.L. performed the CRISPR-based screen. Epilipidomics analysis were performed by P.N. and M.F. FENIX assays and corresponding LC/MS/MS and UV/Vis experiments were performed by O.Z., E.L.S. and I.E. with support from D.A.P. L.P. and A.G.S. contributed to the study of truncated vesicles permeabilization and studies using PhotoPC. Synthesis and characterization of PhotoPC was performed by M.B.S. and D.B.K. D.C. synthesized ent-cholesterol. F.G. and L.E.S.N performed and analysed the yeast spot assays. B.M. carried the analysis determining selenium content. H.A. designed and conducted in vivo experiments, followed by the implementation of related analyses. C.K., N.A., K.K. and B.K. assisted with in vivo experiments and subsequent analyses. F.P.F, V.K. and K.B. were responsible for performing and analysing the MM1S xenograft experiments. A.H. and P.I. synthesize and characterized the specificity of DHCR7 inhibitor RB38. T.C.G.M. and K.M. performed the quantification of 7-DHC oxidation products. W.S. contributed with lipidomics and sterol detections and analysis. L.K. and J.K.S. conducted structural modelling. M.C., G.W.B., A.T., R.C.B., S.D., S.M., A.W., M.K. and I.W. contributed with reagent, critical information and/or platforms. J.P.F.A. initiated, supervised the study and conceived the experimental plan. All authors contributed with discussion and data interpretation and read and agreed on the content of the paper.

Competing interests The authors declare no competing interests.

Additional information

Supplementary information The online version contains supplementary material available at https://doi.org/10.1038/s41586-023-06878-9.

Correspondence and requests for materials should be addressed to José Pedro Friedmann Angeli.

Peer review information *Nature* thanks Andreas Linkermann, Markus Müschen, Ned Porter and the other, anonymous, reviewer(s) for their contribution to the peer review of this work. Peer reviewer reports are available.

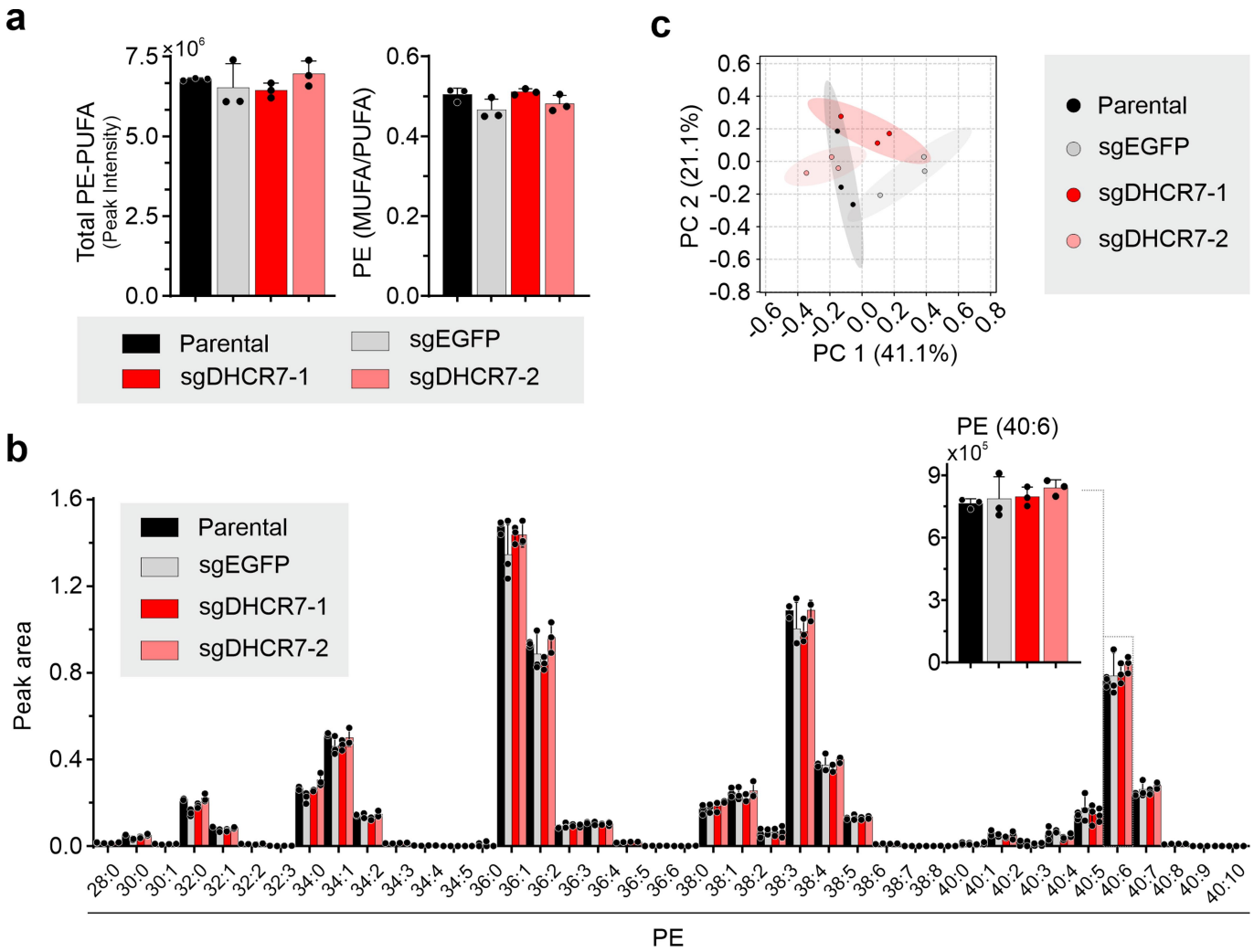

Extended Data Fig. 1 | Lipidomic characterization of DHCR7-deficient cells. **a**, Lipidomics analysis of HT1080 cells expressing a Cas9 containing lentiviral vector co-expressing sgRNA targeting *DHCR7* or *EGFP* as a control. Represented are the total amount of PE containing PUFA and the ratio of mono- to polyunsaturated fatty acids (MUFA/PUFA) in PE species. Data are represented as mean values ± s.d. of n = 3 technical replicates (from 10 cm plate) performed once. **b**, Fatty acid composition of PE species in the indicated cell lines. Data are representative of mean values ± s.d. of n = 3 technical replicates (6 cm plate) performed twice. **c**, Principal component analysis of PE composition data.

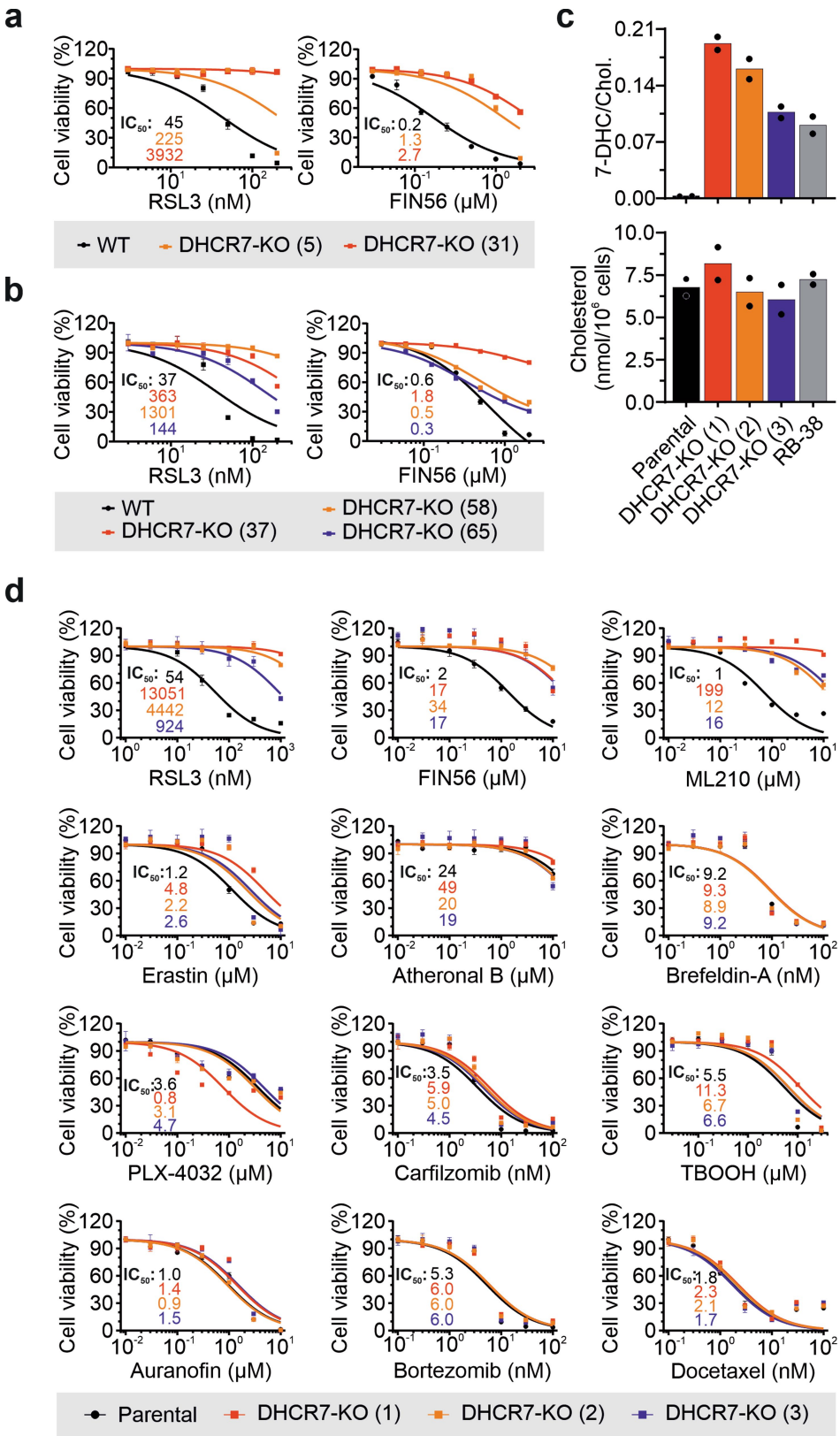

Extended Data Fig. 2 | DHCR7 deficiency impact on ferroptosis and other cell death modalities. a and **b**, Dose-dependent toxicity of RSL3 and FIN56 in *DHCR7*-Knockout clonal cell lines generated in the HT1080 (a) and PFa1 (b) cell lines. **c**, Levels of 7-DHC in MDA-MB-435 parental lines untreated and treated with a DHCR7 inhibitor (RB38 [500 nM]) and three independent *DHCR7*-KO clones. Data are represented as mean values ± s.d. of n = 2 technical replicates (from 10 cm plate) performed once. **d**, Dose-dependent toxicity of RSL3, FIN56, ML210, Erastin, Atheronal, Brefeldin-A, PLX-4032, Carfilzomib, TBOOH, Auranofin; Bortezomib and Docetaxel in MDA-MB-435 parental cells and the three DHCR7 knockout clones. Cell viability was assessed after 48 h using Alamar blue and data are representative of mean ± s.d. of n = 3 technical replicates of 2 independent experiments.

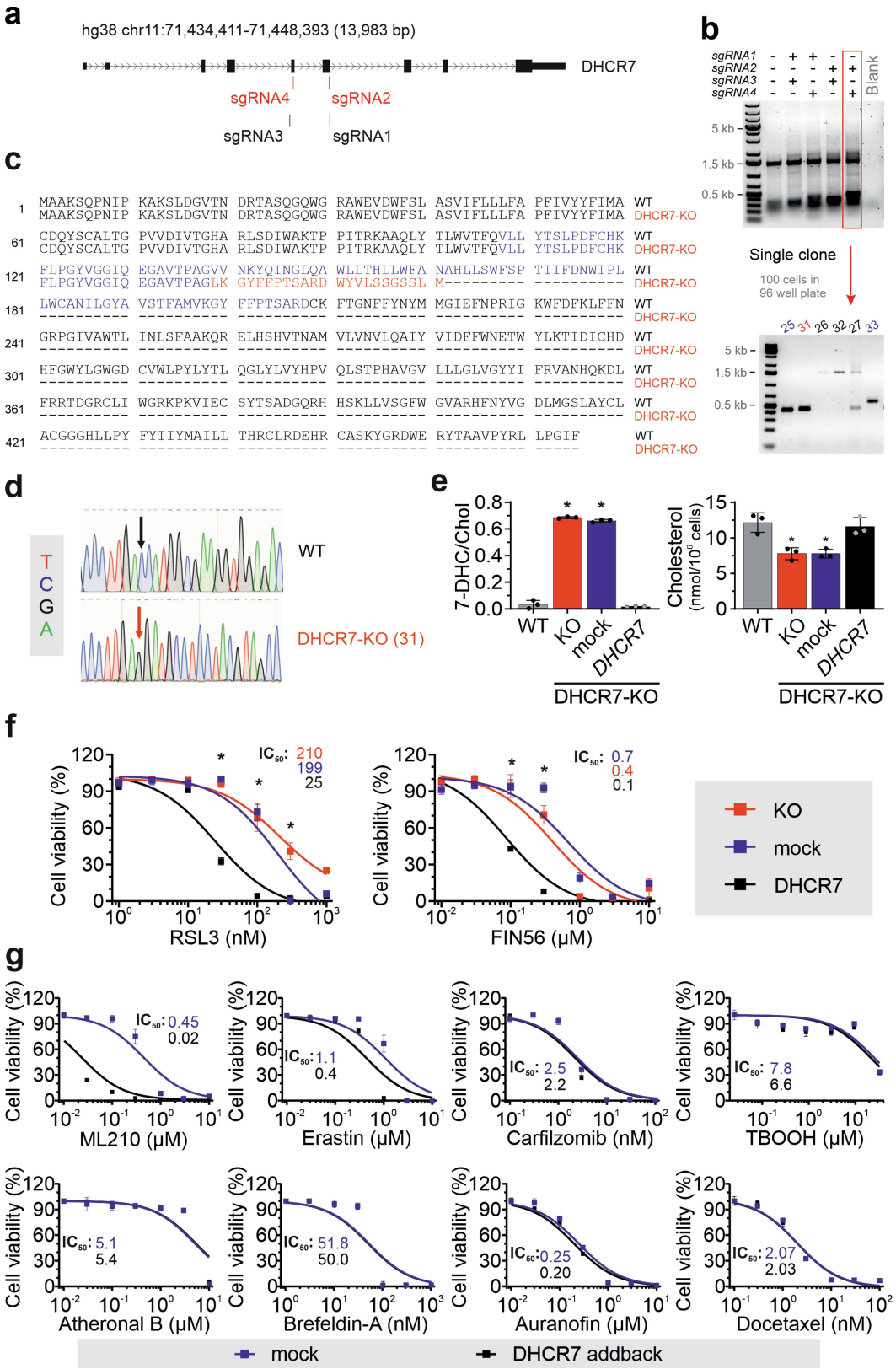

Extended Data Fig. 3 | See next page for caption.

Extended Data Fig. 3 | Characterization of HT1080 DHCR7-deficient clonal cell line. a, Graphical representation of the strategy used to generate DHCR7-deficient cells with defined genomic alterations. **b**, Representative PCR of the pools and single clones derived thereof. **c**, Schematic representation of the sequencing results obtained from the PCR product (in blue) covering the edited region (in red) in comparison with the wild-type product. **d**, Sequencing chromatogram obtained from the edited allele. **e**, Relative quantification of 7-DHC and levels of Cholesterol in HT1080 Cas9 WT, *DHCR7*-Knockout clone (DHCR7-KO) and the corresponding DHCR7-KO reconstituted with an empty lentiviral vector (mock) or overexpressing DHCR7. Data are the mean ± s.d. of n = 3 wells of a 6-well plate from one representative experiment. **f**, Dose-dependent toxicity of RSL3 and FIN56 in HT1080 Cas9 DHCR7-KO clone and overexpressing DHCR7 or mock. **g**, Dose-dependent toxicity of ML210, Erastin, Carfilzomib, TBOOH, Atheronal B, Brefeldin-A, Auranofin and Docetaxel in HT1080 Cas9 DHCR7-KO clone transduced with a mock or a DHCR7 expressing vector. Cell viability was assessed after 48 h using Alamar blue and data are representative of mean ± s.d. of n = 3 technical replicates 2 independent experiments. *$p < 0.05$; two-way ANOVA (e, f).

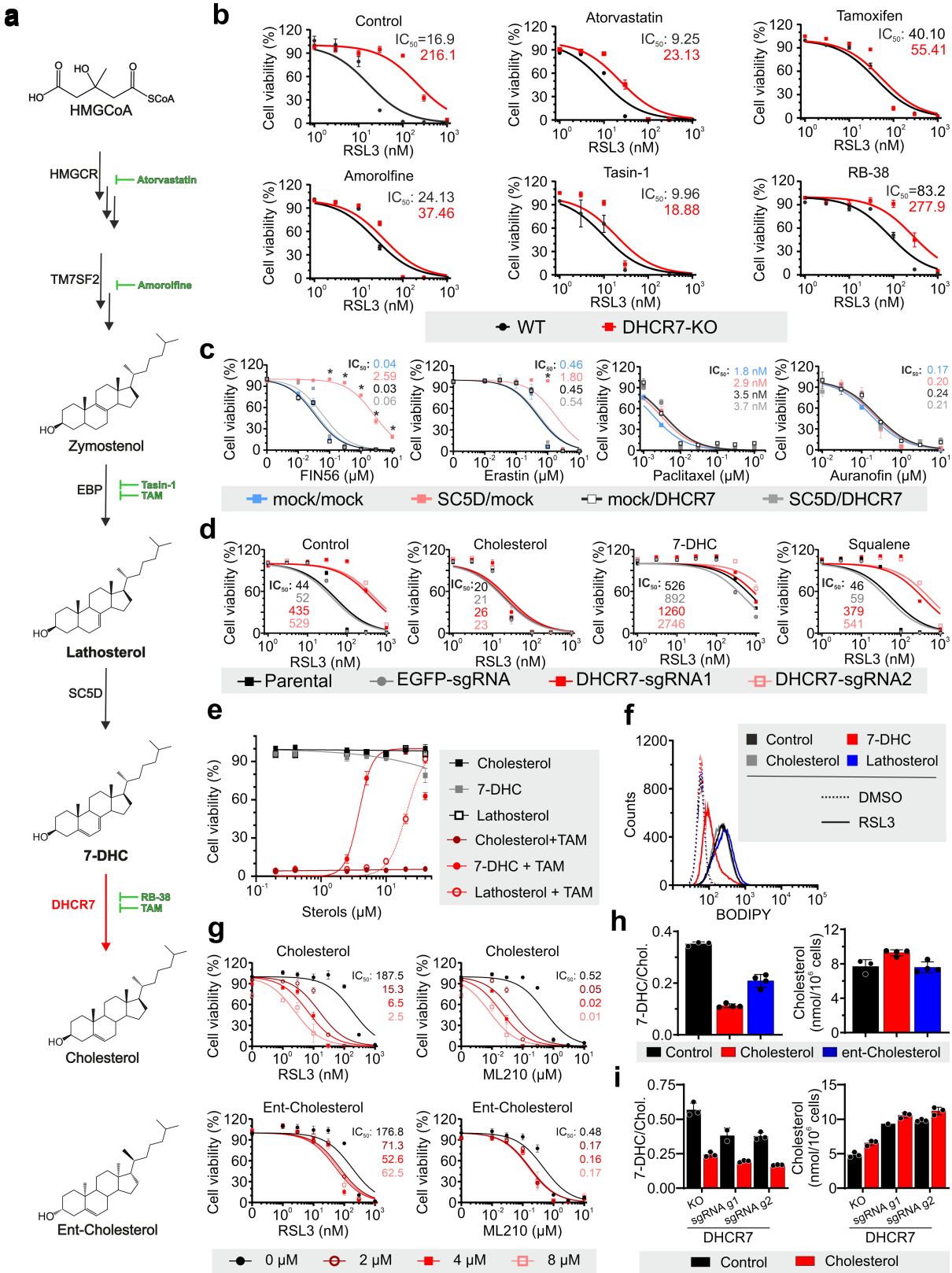

Extended Data Fig. 4 | See next page for caption.

Extended Data Fig. 4 | Impact of 7-DHC accumulation on ferroptosis. **a**, Schematic depiction of cholesterol biosynthesis, highlighting the pharmacological targets of the enzymes used in the present work. **b**, Dose-dependent toxicity of RSL3 in DHCR7 WT and knockout HT1080 cells in the presence of pharmacological agents modulating cholesterol biosynthesis. Concentrations for the different inhibitors are: atorvastatin [1 μM], Amorolfine [500 nM], Tasin-1 [500 nM], Tamoxifen [1 μM] and RB38 [500 nM]. **c**, Dose-dependent toxicity of Paclitaxel and Auranofin in HT1080 Cas9 *DHCR7/SC5D* knockout transduced with *SC5D* and/or *DHCR7*. **d**, Effect of sterols and squalene supplementation (10 μM) on RSL3 toxicity in cell expressing a control and two independent sgRNA targeting DHCR7. **e**, Effect of sterol supplementation on a genetic model of Gpx4 deficiency, i.e Pfa1 cells treated with TAM. **f**, Flow cytometry analysis of BODIPY 581/591 C11 oxidation in HT1080 cell line induced by RSL3 treatment ([100 nM], 5 h) in cells pretreated for 16 h with 10 μM of different sterols. **g**, Impact of exogenous free cholesterol and ent-cholesterol on the sensitivity of DHCR7-deficient cells to GPX4 inhibitors. **h**, Relative quantification of 7-DHC and Cholesterol levels in DHCR7-deficient cells treated with cholesterol and ent-cholesterol (8 μM). **i**, 7-DHC levels in HT1080 Cas9 DHCR7-KO clone and pool of HT1080 expressing two independent sgRNA targeting DHCR7 treated with Cholesterol (5 μM). Data are representative data of mean ± s.d. of n = 3 technical replicate of a 96-well plate (b-e) or 6-well (f-i) performed twice. Cell viability was assessed after 48 h (b-d) or 72 h (e, f) using Alamar blue and data are representative of mean ± s.d. of n = 3 technical replicates (96-well plate) performed three times.

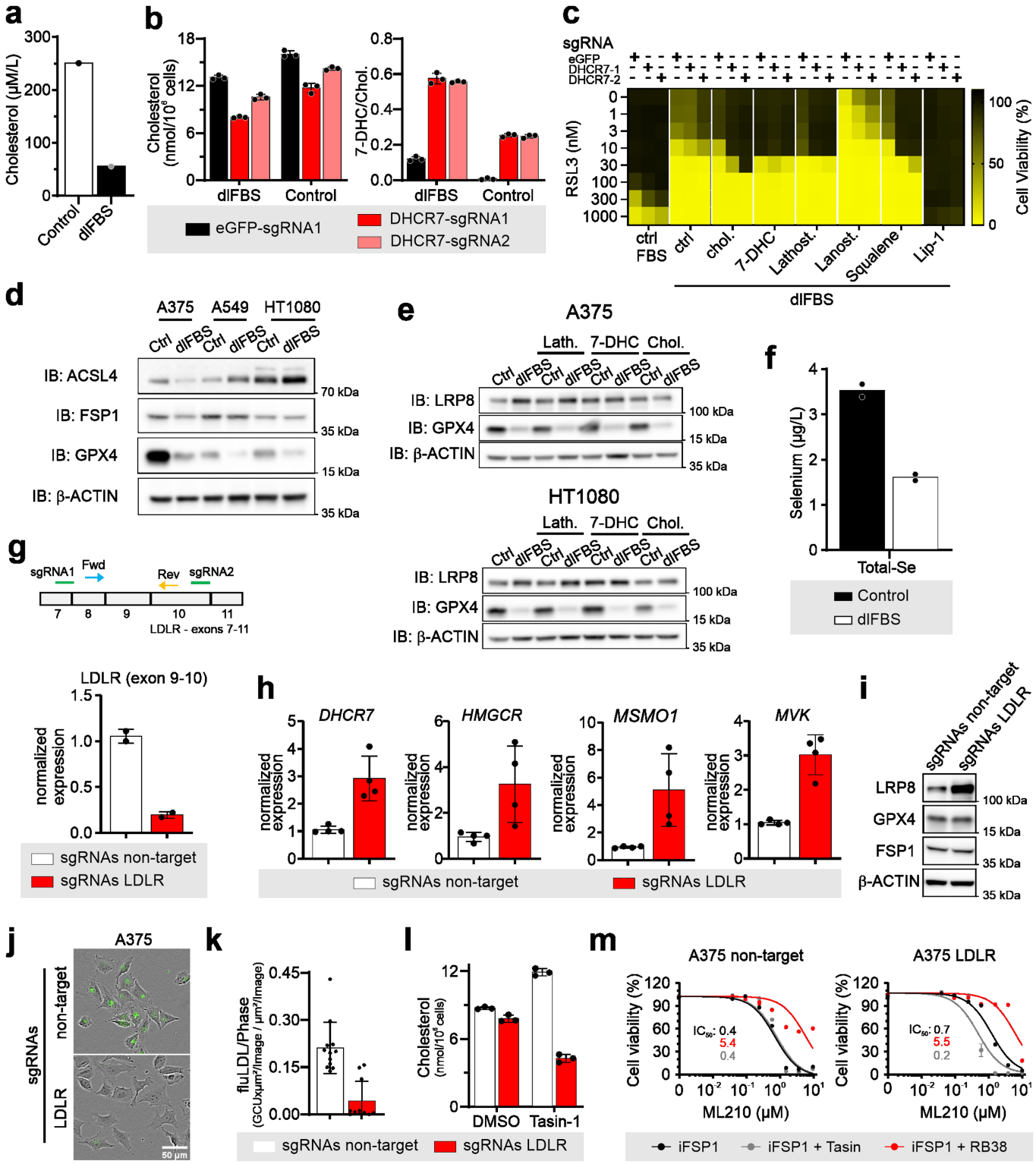

Extended Data Fig. 5 | See next page for caption.

Extended Data Fig. 5 | Influence of cholesterol low conditions on the antiferroptotic activity of the 7-DHC/DHCR7 axis. a, Quantification of cholesterol in FBS samples treated with fumed silica (20 g/L). Results are representative of one batch preparation used throughout this experiments. **b**, Relative quantification of 7-DHC and Cholesterol levels in HT1080 cells expressing a control and a DHCR7 targeting sgRNA grown in normal and delipidated FBS (dlFBS). **c**, Assessment of the response to RSL3 of DHCR7-deficient and proficient cells in FBS and dlFBS containing the indicated metabolites. **d**, Immunoblot analysis of ferroptosis regulators, FSP1, ACSL4 and GPX4 in cells grown in FBS and dlFBS. **e**, Immunoblot analysis of LRP8 and GPX4 in the indicated cell lines grown in FBS and dlFBS in the presence of the specified sterols (10 μM, 48 h). **f**, Total quantification of selenium by ICP-MS in FBS and dlFBS. **g**, Strategy and validation of A375 LDLR-KO cell lines using primers specific for the LDLR transcript. **h**, Assessment of SREBP2 target genes (DHCR7, HMGR, MSMO1 and MVK) in LDLR proficient and deficient cells. **i**, Immunoblot of LRP8 and GPX4 in the indicated cell lines. **j**, Assessment of uptake capacity of fluorescently labelled LDL in LDLR proficient and deficient cells. Visualization (**j**) and quantification of LDL (**k**) or cholesterol upon Tasin-1 (500 nM) treatment for 48 h (**l**) in LDLR proficient and deficient cells. **m**, Effect of LDLR loss on ferroptosis induction (ML210 + 2 μM iFSP1) in RB38 (500 nM) and Tasin-1 (500 nM) treated cells. Data are representative of mean ± s.d. of n = 2 (f, g), n = 3 (b, c, l, m), n = 4 (h) or n = 12 (k) technical replicates of a 96-well plate (c, m, j, k) or 6-well plate (b, g, h, l, m) performed twice. Cell viability was assessed after 72 h using Alamar blue (c, m).

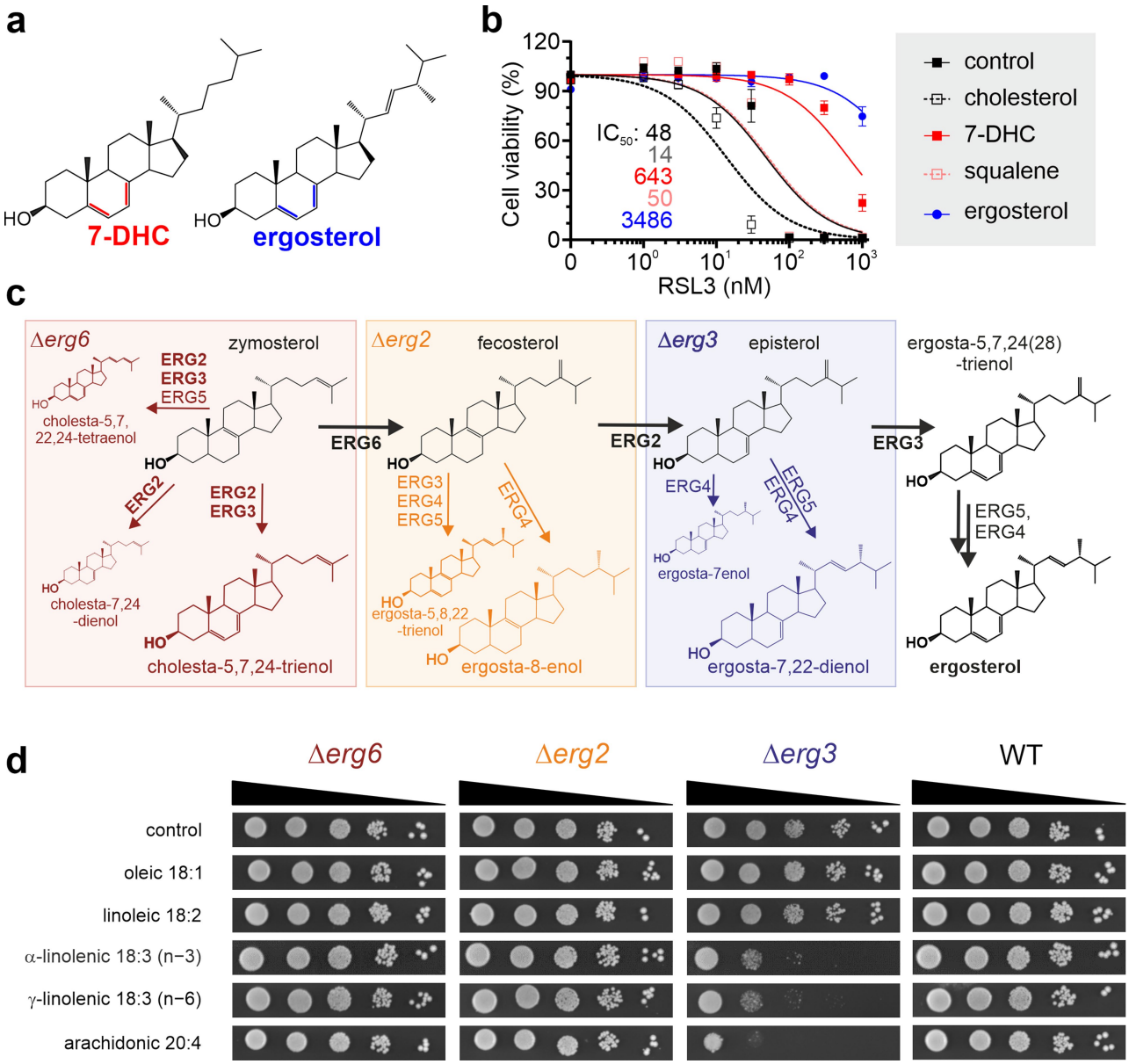

Extended Data Fig. 6 | Role of B-ring unsaturated sterol in ferroptosis. **a**, Chemical structure of 7-DHC and ergosterol highlighting the conjugated double-bond. **b**, Effect of sterols and squalene supplementation (5 µM) on RSL3-induced cell death in the HT1080 cell line. Cell viability was assessed after 48 h using Alamar blue, data are representative of mean ± s.d. of n = 3 technical replicates from one representative of 2 independent experiments. **c**, Schematic representation of the ergosterol biosynthesis pathway in *S. cerevisae*, highlighting the major products reported to accumulate in these strains. **d**, Spot dilutions of the indicated strains of *S. cerevisiae* treated with the designated PUFAs (50 µM).

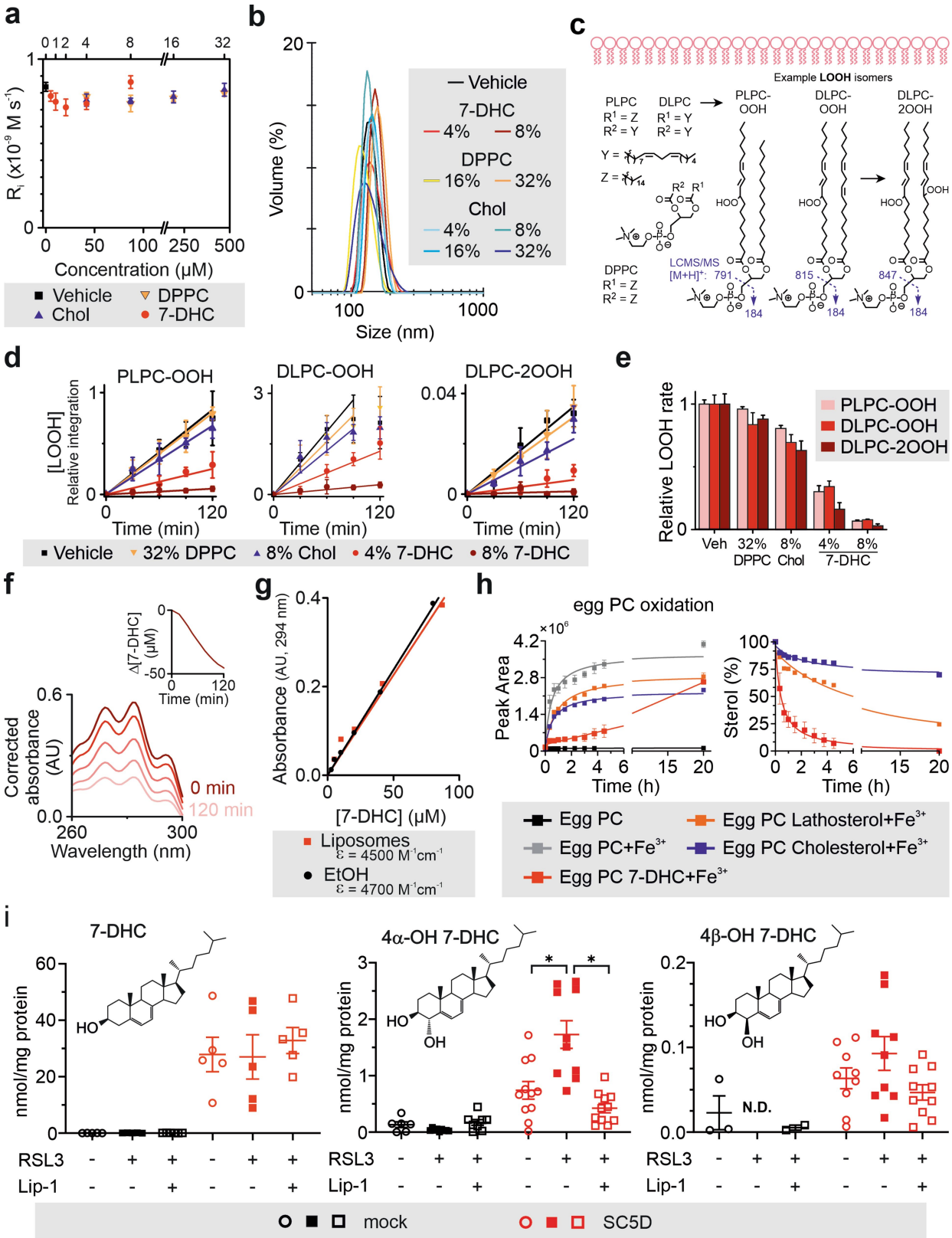

Extended Data Fig. 7 | See next page for caption.

Extended Data Fig. 7 | Impact and consequence of 7-DHC on phospholipid peroxidation. a, Rate of initiation (R_i) in each soy PC liposome composition. **b**, Dynamic light scattering assessment of the impact of different sterols on the integrity of liposomes **c**, Scheme of the formation of PLPC-OOH, DLPC-OOH and DLPC-2OOH during autoxidation of soy PC that can be analysed by LC-MS/MS using MRM. **d**, The resulting profiles of PLPC-OOH, DLPC-OOH and DLPC-2OOH formation over time (integrations are relative to an internal standard (prostaglandin B2). **e**, Calculated rates from linear regression of the data related to d. **f**, Representative UV-Vis spectra obtained from a sample of soy PC with 8 mol% 7-DHC during autoxidation. Spectra were processed by subtracting the background trace of vehicle liposomes immediately after the addition of DTUN. Loss of 7-DHC was plotted from the 294 nm peak (inset) with concentrations determined from a standard curve from liposomes prepared with soy PC with inhibitor and added 7-DHC (see Supporting Information). **g**, Standard curve for 7-DHC prepared in either 95% EtOH or in soy PC liposomes with inhibitor. **h**, Time course of iron/ascorbate mediated oxidation of Egg-PC and sterol consumption in liposomes containing cholesterol, lathosterol or 7-DHC monitored via HPLC-UV detection (235 nm for PCOOH, 205 nm for cholesterol and lathosterol and 275 nm for 7-DHC). **i**, Quantification of 7-DHC and secondary oxidation products of 7-DHC in HT1080 SC5D/DHCR7 knockout cells expressing empty vector (black) and SC5D (red) upon 200 nM RSL3 with and without 500 nM Lip1 (6 h). Data are the mean ± s.d of n = 6 wells of a 10 cm plate from two independent experiments, *$p < 0.05$ two-way ANOVA (i). Each reaction (b, d, e, f, h) was repeated three times and is reported as the mean ± s.d for the kinetic plot (d) or error propagation from the slopes of d derived from linear regression.

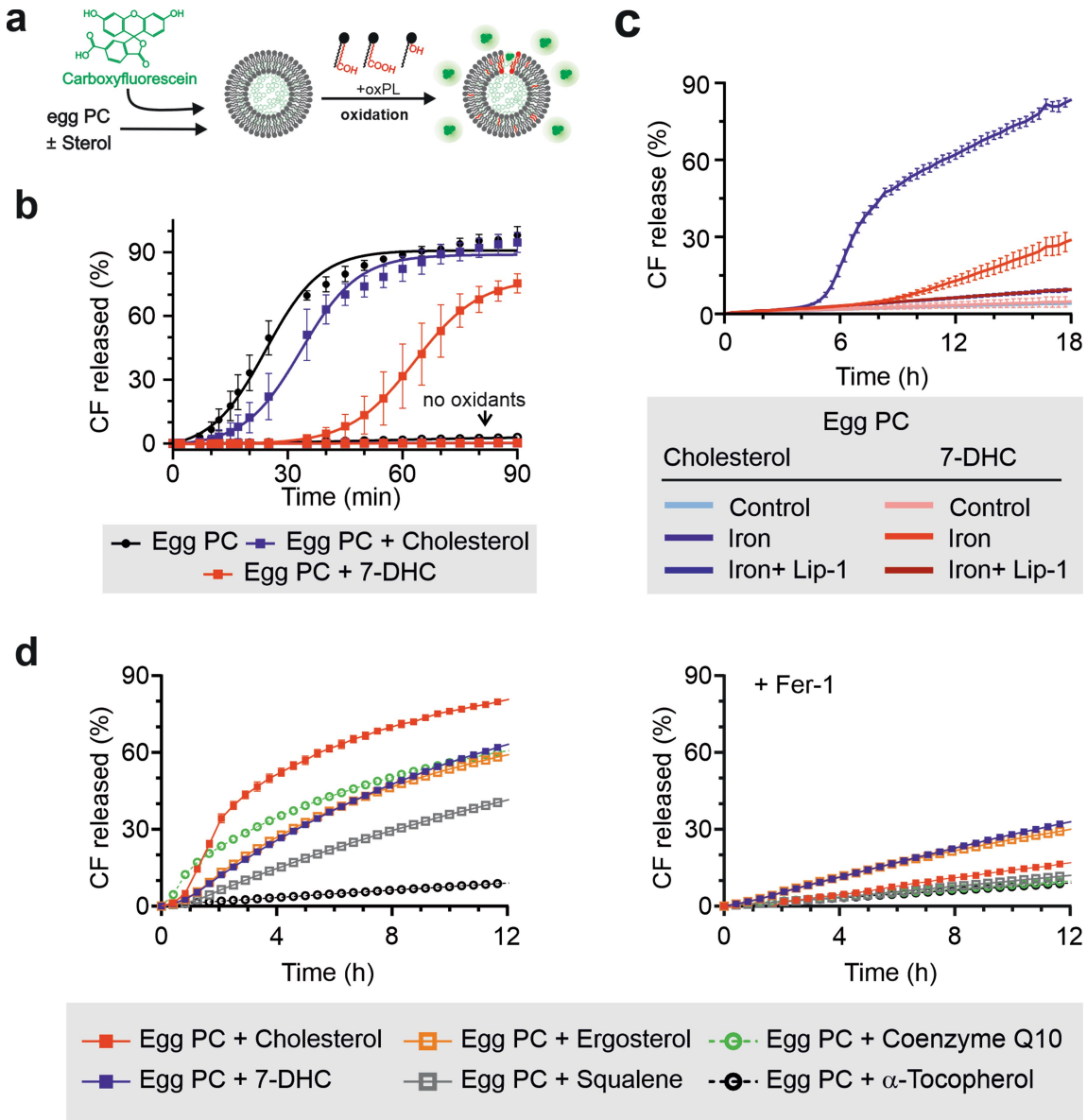

Extended Data Fig. 8 | Impact of ferroptosis inhibitors on oxidant mediated liposomal rupture. a, Schematic representation of the CF/liposome assay used to monitor vesicle permeability. **b**, CF release from CF encapsulated liposomes generated using different sterols. CF release was stimulated using a mixture of iron and ascorbate (10 µM and 100 µM respectively). **c**, Impact of Lip1 on CF release from CF encapsulated liposomes containing cholesterol or 7-DHC. **d**, CF release in vesicles containing different ferroptosis inhibitors (10 µM) stimulated using a mixture of iron and ascorbate (20 µM and 200 µM respectively) in the absence (left panel) or in the presence of Ferrostatin-1 (Fer-1; right panel). Data are representative of mean ± s.d. of n = 3 technical replicates of 2 independent experiments.

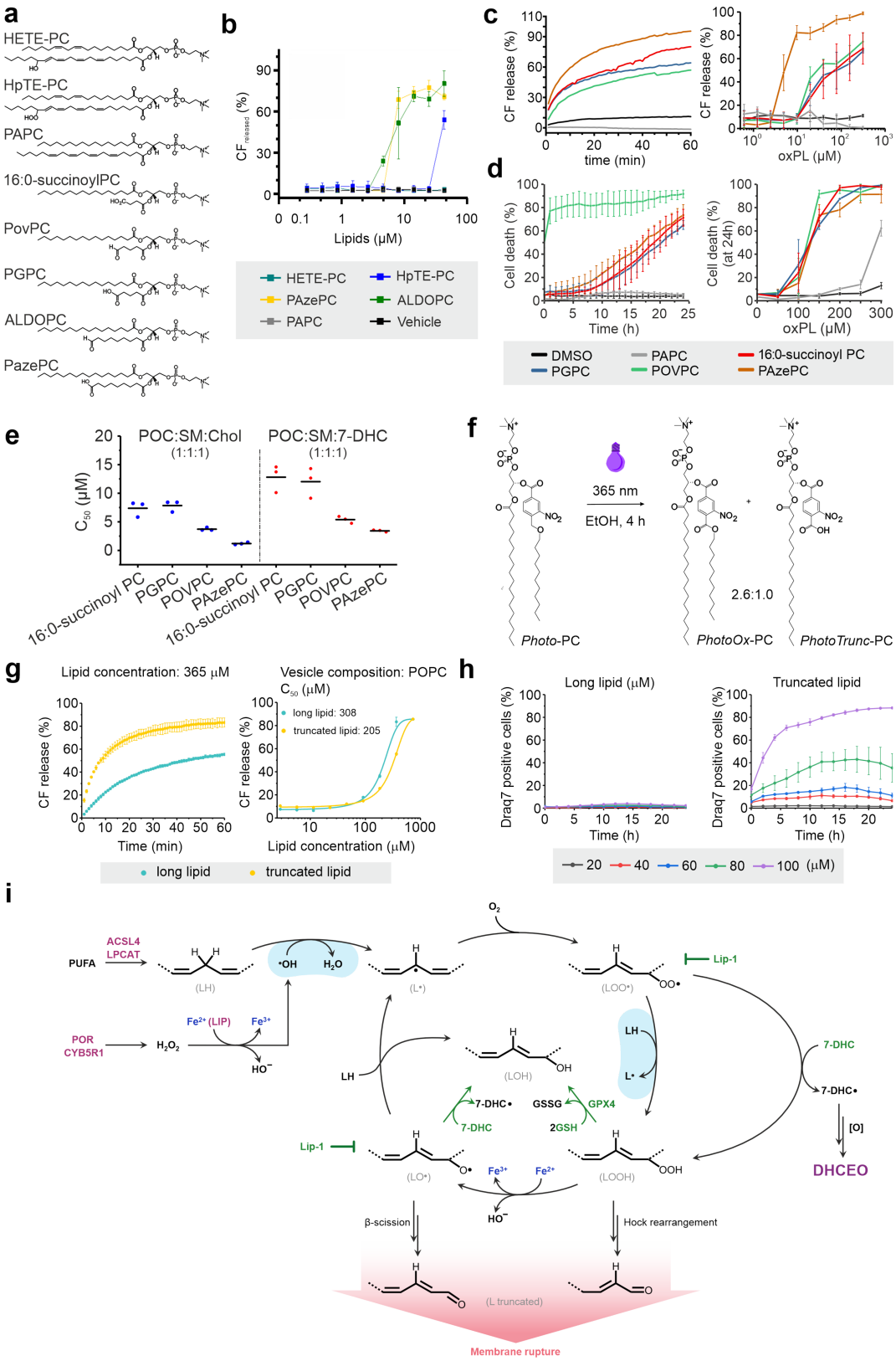

Extended Data Fig. 9 | See next page for caption.

Extended Data Fig. 9 | Role of truncated phospholipid in membrane permeability. a, Structure of selected truncated PC and related molecules tested. **b** Impact of native, peroxidised and truncated PC species in CF permeabilization. **c**, CF release in liposomes treated with different PC truncated species in a time and dose-dependent manner. **d**, Cell death induction by different PC truncated species in HT1080 cells in a time and dose-dependent manner. **e**, C50 of different truncated PL on CF release from liposomes containing 7-DHC or cholesterol. **f**, Schematic representation for the chemical basis of the PhotoPC probe: photoactivation leads to the generation of a defined mixture between the oxidized derivative PhotoOx-PC and the truncated derivative PhotoTrunc-PC. **g**, CF release in liposomes treated with PhotoPC before and after photoactivation in response to dose (fixed 1 h exposure) and time (fixed 365 μM). **h**, assessment of cell death (Draq7 positive) induced by equimolar concentrations of PhotoPC and PhotoTrunc-PC in HT1080 cells. Data are the mean ± s.d. of n = 6 wells of a 96-well plate from one representative of two independent experiments. **i**, Schematic representations of the events leading to the formation of truncated phospholipid species of formation of oxidatively truncated (phospho)lipid species and 7-DHC impact on it. Proferroptotic players are depicted in red and suppressing events are depicted in green.

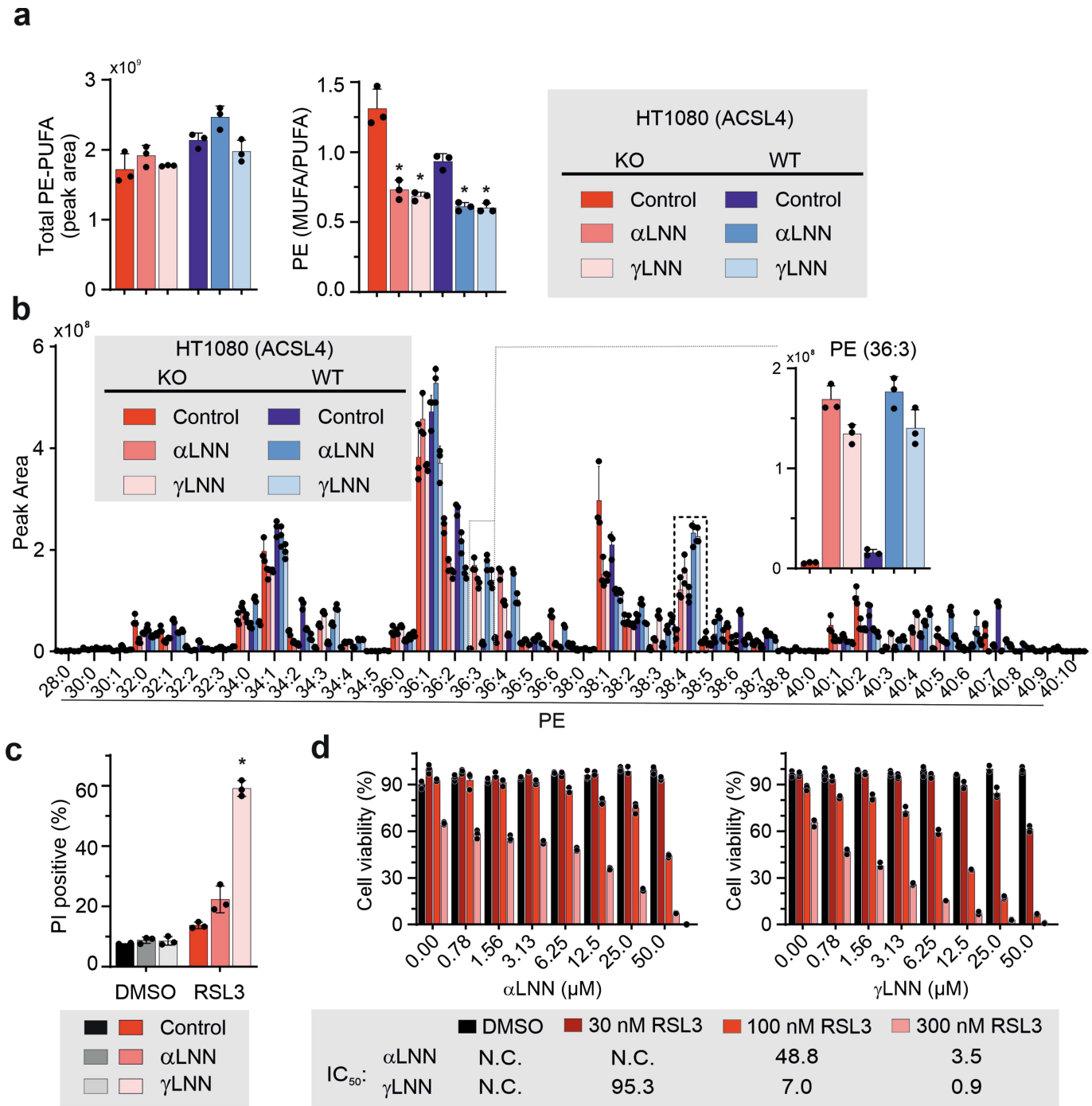

Extended Data Fig. 10 | Conjugation at the omega position affects ferroptosis sensitivity. a, Lipidomics analysis of WT and *ACSL4* KO HT1080 cell lines incubated for 16 h with αLNN and γLNN (20 μM). Presented are the total amount of PE containing PUFA and the ratio of mono- to polyunsaturated fatty acids (MUFA/PUFA) in PE species. Mean values ± s.d. of n = 3 technical replicates (10 cm plate) performed twice. **b**, Fatty acid composition of PE species in WT and *ACSL4* KO HT1080 cell lines incubated for 16 h with αLNN and γLNN (20 μM). Mean values ± s.d. of n = 3 technical replicates (10 cm plate) performed twice. **c**, Assessment of the impact of αLNN and γLNN [20 μM] re-senitization on RSL3-induced ferroptosis. Cell viability was assessed after 24 h measuring PI incorporation. Mean values ± s.d. of n = 3 technical replicates (6 cm plate) performed twice are presented. **d**. Dose-dependent effect of α-LNN and γ-LNN on RSL3 mediated toxicity in HT1080 *ACSL4* KO cell lines. Data are the mean ± s.d. of n = 6 wells of a 96-well plate from one representative of two independent experiments. *p < 0.05; two-way ANOVA.

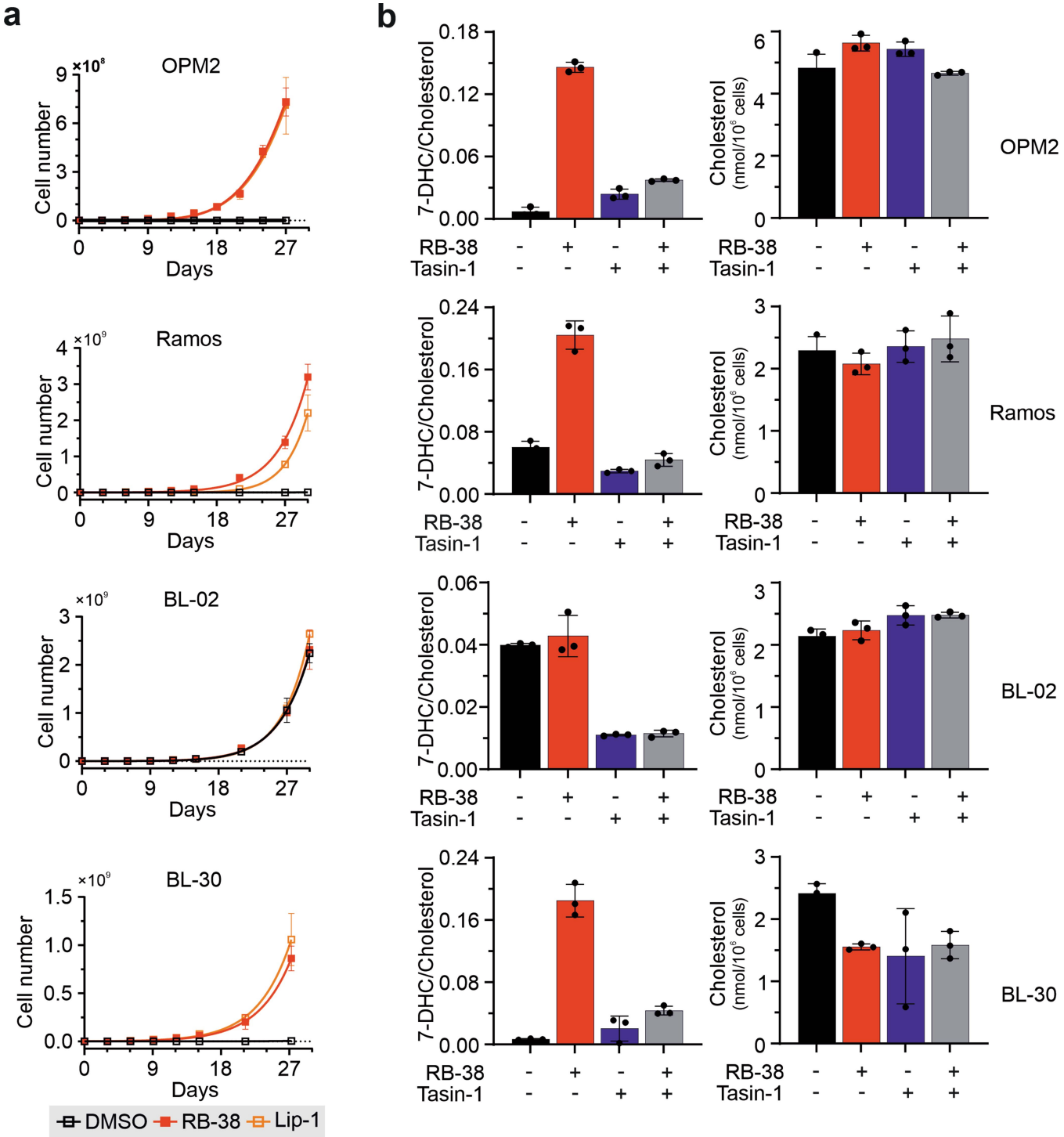

Extended Data Fig. 11 | Impact of 7-DHC accumulation on BL growth. **a**, Impact of selected pharmacological inhibitors of DHCR7 (RB38) and Lip1 on Multiple Myeloma cell line OPM2 and the BL cell lines RAMOS, BL02 and BL30 grown in the absence of thiols and pyruvate. **b**, Relative quantification of 7-DHC and cholesterol levels in cell lines treated with RB38 and Tasin-1. Data are the mean ± s.d. of n = 3 wells, of a 6-well plate from one representative experiment.

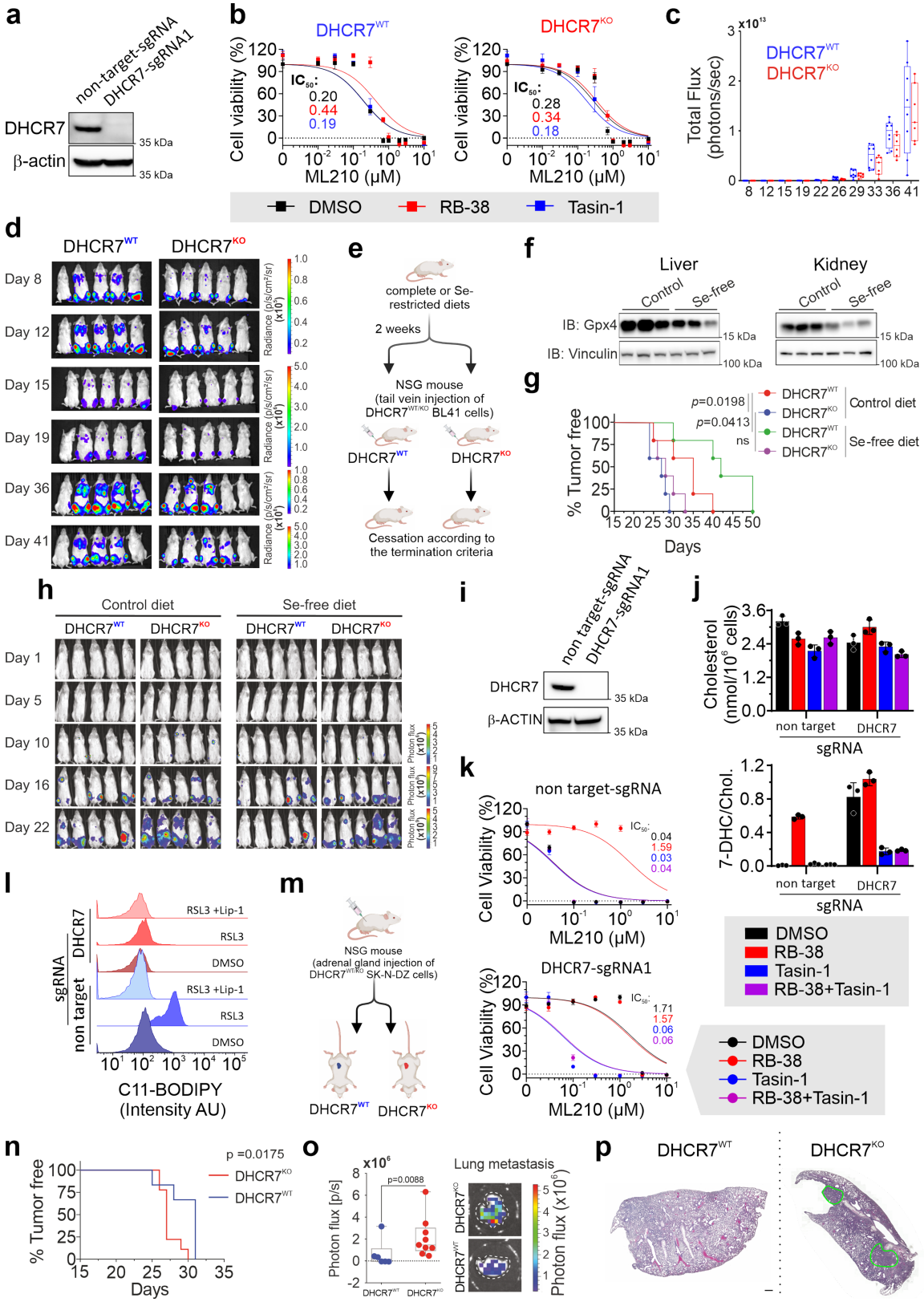

Extended Data Fig. 12 | See next page for caption.

Extended Data Fig. 12 | Impact of DHCR7 loss in vivo. a, Immunoblot for DHCR7 in MM1S cells DHCR7-proficient and deficient. Representative of n = 2. **b**, Dose-dependent toxicity of ML210 in $DHCR7^{WT}$ or $DHCR7^{KO}$ in the presence of indicated treatments. **c**, Tumour growth upon implantation of MM1S $DHCR7^{WT}$ (n = 10) or $DHCR7^{KO}$ (n = 10). Data are mean ± SEM; p value n.s., Mann–Whitney test one-tailed. In each box, horizontal lines denote mean values, while the box contains the 25th to 75th percentiles of dataset and whiskers mark the 5th and 95th percentiles. **d**, Representative luminescence images of mice from c. **e**, Schematic of tail vein injection of $DHCR7^{WT}$ (n = 5) or $DHCR7^{KO}$ (n = 5) BL41 cell in mice under selenium-adequate or -deprived diet. **f**, Immunoblot for GPX4 from tissues of animals related to e. **g**, Kaplan–Meier plot displaying tumour-free survival (TFS) for mice injected with $DHCR7^{WT}$ (n = 5) or $DHCR7^{KO}$ (n = 5) BL41 cells. Data represent the mean ± s.e.m.; Mann–Whitney test one-tailed; A Log-rank (Mantel–Cox) test was conducted for statistical analysis, p values are indicated. **h**, Luminescence images related to g. **i**, Immunoblot for DHCR7 in SK-N-DZ $DHCR7^{KO}$ and $DHCR7^{WT}$. **j**, Relative quantification of cholesterol and 7-DHC levels in SK-N-DZ cells treated with RB38 and Tasin-1. Data are the mean ± s.d. of n = 3 wells from one representative experiment. **k**, Dose-dependent toxicity of ML210 in the indicated cells. **l**, Flow cytometry analysis of BODIPY 581/591 C11 oxidation in SK-N-DZ cells induced by RSL3 treatment ([100 nM], 3 h) and Lip1 500 nM. **m**, Schematic representation illustrates an orthotopic mouse model created by transplanting $DHCR7^{WT}$ or $DHCR7^{KO}$ SK-N-DZ cells into the right adrenal gland of NSG mice. **n**, Kaplan- Meier plot displaying TFS for mice injected orthotopically with $DHCR7^{WT}$ (blue, n = 6) or $DHCR7^{KO}$ (red, n = 9) SK-N-DZ cells; *p < 0.05, A Log-rank (Mantel–Cox) test was conducted for statistical analysis. **o**, Lung colonization was evaluated (left panel) in mice orthotopically transplanted with SK-N-DZ neuroblastoma cells, with $DHCR7^{WT}$ (red, n = 6) or $DHCR7^{KO}$ (blue, n = 9), using ex vivo lung bioluminescence analysis (right panel);. **p**, Representative examples of evidence of metastases from o (indicated by green circle lines), determined by Hematoxylin and Eosin staining from samples of n. Scale bar: 500 µM. Cell viabilities were assessed after 72 h using Alamar blue, data are mean ± s.d. of n = 3 replicates from one representative of three independent experiments (b, k). RB38 (500 nM) and Tasin-1 (500 nM) (b, j, k). Panels created with BioRender.com (e, m).

nature portfolio

Corresponding author(s): Dr. José Pedro Friedmann Angeli

Last updated by author(s): Sep 3, 2023

Reporting Summary

Nature Portfolio wishes to improve the reproducibility of the work that we publish. This form provides structure for consistency and transparency in reporting. For further information on Nature Portfolio policies, see our Editorial Policies and the Editorial Policy Checklist.

Statistics

For all statistical analyses, confirm that the following items are present in the figure legend, table legend, main text, or Methods section.

n/a	Confirmed
☐	☒ The exact sample size (*n*) for each experimental group/condition, given as a discrete number and unit of measurement
☐	☒ A statement on whether measurements were taken from distinct samples or whether the same sample was measured repeatedly
☐	☒ The statistical test(s) used AND whether they are one- or two-sided *Only common tests should be described solely by name; describe more complex techniques in the Methods section.*
☐	☒ A description of all covariates tested
☐	☒ A description of any assumptions or corrections, such as tests of normality and adjustment for multiple comparisons
☐	☒ A full description of the statistical parameters including central tendency (e.g. means) or other basic estimates (e.g. regression coefficient) AND variation (e.g. standard deviation) or associated estimates of uncertainty (e.g. confidence intervals)
☒	☐ For null hypothesis testing, the test statistic (e.g. *F*, *t*, *r*) with confidence intervals, effect sizes, degrees of freedom and *P* value noted *Give P values as exact values whenever suitable.*
☒	☐ For Bayesian analysis, information on the choice of priors and Markov chain Monte Carlo settings
☒	☐ For hierarchical and complex designs, identification of the appropriate level for tests and full reporting of outcomes
☒	☐ Estimates of effect sizes (e.g. Cohen's *d*, Pearson's *r*), indicating how they were calculated

Our web collection on statistics for biologists contains articles on many of the points above.

Software and code

Policy information about availability of computer code

Data collection	SnapGene viewer 5.2.4, Coreldraw 2019 21.0.0.593, BD FACSDiva 6.1.3, Flowing software 2.5.1, SparkControl V2.1 (Tecan), SWISS-MODEL (https://swissmodel.expasy.org/); NetPhos 3.1 server (http://www.cbs.dtu.dk/services/NetPhos/); PyMOL 2.3.4; Skyline v. 21.1.0.146 (MacCoss Lab15); MetaboAnalyst online platform (https://www.metaboanalyst.ca); Genesis v. 1.8.1 (Bioinformatics TU-Graz17); LipidLynxX system (https://www.biorxiv.org/content/10.1101/2020.04.09.033894v1); TraceFinder V3.3 software (Thermo Scientific, Bremen, Germany);
Data analysis	GraphPad Prism 9.2.0, Origin 9.7.0.188, Microsoft Excel 2016 MSO (16.0.5215.1000), ImageJ 1.53c (https://imagej.nih.gov/ij/);

For manuscripts utilizing custom algorithms or software that are central to the research but not yet described in published literature, software must be made available to editors and reviewers. We strongly encourage code deposition in a community repository (e.g. GitHub). See the Nature Portfolio guidelines for submitting code & software for further information.

Data

Policy information about availability of data

All manuscripts must include a data availability statement. This statement should provide the following information, where applicable:

- Accession codes, unique identifiers, or web links for publicly available datasets
- A description of any restrictions on data availability
- For clinical datasets or third party data, please ensure that the statement adheres to our policy

The datasets generated during and/or analysed during the current study are available from the corresponding author upon reasonable request.

Human research participants

Policy information about studies involving human research participants and Sex and Gender in Research.

Reporting on sex and gender	*Use the terms sex (biological attribute) and gender (shaped by social and cultural circumstances) carefully in order to avoid confusing both terms. Indicate if findings apply to only one sex or gender; describe whether sex and gender were considered in study design whether sex and/or gender was determined based on self-reporting or assigned and methods used. Provide in the source data disaggregated sex and gender data where this information has been collected, and consent has been obtained for sharing of individual-level data; provide overall numbers in this Reporting Summary. Please state if this information has not been collected. Report sex- and gender-based analyses where performed, justify reasons for lack of sex- and gender-based analysis.*
Population characteristics	*Describe the covariate-relevant population characteristics of the human research participants (e.g. age, genotypic information, past and current diagnosis and treatment categories). If you filled out the behavioural & social sciences study design questions and have nothing to add here, write "See above."*
Recruitment	*Describe how participants were recruited. Outline any potential self-selection bias or other biases that may be present and how these are likely to impact results.*
Ethics oversight	*Identify the organization(s) that approved the study protocol.*

Note that full information on the approval of the study protocol must also be provided in the manuscript.

Field-specific reporting

Please select the one below that is the best fit for your research. If you are not sure, read the appropriate sections before making your selection.

☒ Life sciences ☐ Behavioural & social sciences ☐ Ecological, evolutionary & environmental sciences

For a reference copy of the document with all sections, see nature.com/documents/nr-reporting-summary-flat.pdf

Life sciences study design

All studies must disclose on these points even when the disclosure is negative.

Sample size	no samples size calculation was performed. Preliminary cell viability experiments showed small variations between biological replicates, so we chose n ≥3 for reproducibility. For the determination of phospholipid composition we chose n ≥ 3 according to our experience in previos experiments (small variation between biological replicates)
Data exclusions	In very rare cases single values of biological triplicates were excluded from the analysis due to te cell clumps/uneven plating.
Replication	All attempts to replicate experiments were successful, accounting for the robustness of the results. To guarantee reliable replication of our results we pretested all used sera for their suitability for ferroptosis research. It is know that differing, cholesterol,. vitamin E and selenium concentrations in different sera batches profoundly impact on the outcome of ferroptosis inducing/inhibiting conditions.
Randomization	Randomization was not necessary once cells were injected subcutaneously on the right and left flanks of each mice.
Blinding	Genotypes of the cells injected on both flanks of mice were kept blinded

Reporting for specific materials, systems and methods

We require information from authors about some types of materials, experimental systems and methods used in many studies. Here, indicate whether each material, system or method listed is relevant to your study. If you are not sure if a list item applies to your research, read the appropriate section before selecting a response.

Materials & experimental systems

n/a	Involved in the study
☐	☒ Antibodies
☐	☒ Eukaryotic cell lines
☒	☐ Palaeontology and archaeology
☐	☒ Animals and other organisms
☒	☐ Clinical data
☐	☐ Dual use research of concern

Methods

n/a	Involved in the study
☒	☐ ChIP-seq
☐	☒ Flow cytometry
☒	☐ MRI-based neuroimaging

Antibodies

Antibodies used

Antibodies against antibodies to GPX4 (1:1,000; no. ab125066, Abcam), β-actin (1:10,000; no. A5441, Sigma-Aldrich), ACSL4 (1:200; no. sc-271800, Santa Cruz), Flag-Tag (1:1,000; no. F3165, Sigma-Aldrich), DHCR7 (1:1,000, no. PAS-48204, Invitrogen), LRP8 (1:1000, no.ab108208, abcam); FSP1 (1:10; rat IgG2a monoclonal antibody raised against recombinant human FSP1 protein, clone 6D8-11);

Validation

Antibody against GPX4 (no. ab125066, Abcam) was validated for westernblotting in a previous publication (PMID: 25402683).
Antibody against ACSL4 (no. sc-271800) was validated for westernblotting in a previous publication (PMID: 27842070)
Antibody against β-actin (no. A5441) was validated as loading control for westernblotting in a previous publication (PMID: 15809369)
Antibody against FSP1 was validated for westernblotting in a previous publication (PMID: 31634899)
Antibody against DHCR7 was validated for westernblotting in a previous publication (PMID: 33422461)
ntibody against LRP8 was validated for westernblotting in a previous publication (PMID: 32312520)

Eukaryotic cell lines

Policy information about cell lines and Sex and Gender in Research

Cell line source(s)

4-hydroxytamoxifen (TAM)-inducible Gpx4-/- murine immortalised fibroblasts (Pfa1) have been characterised previously (PMID: 1876024). Human fibrosarcoma (HT1080) cells and human melanoma MB-435S were acquired from ATCC. The multiple myeloma cell line KMS26 was purchased from JCRB. Burkitt lymphoma cell lines were a kind gift of Prof. Gilbert Lenoir (International Agency for Research on Cancer – IARC, Lyon, France).

Authentication

Describe the authentication procedures for each cell line used OR declare that none of the cell lines used were authenticated.

Mycoplasma contamination

Cells are tested at least once a yer for mycoplasm contamination by qPCR at Eurofins Genomics.

Commonly misidentified lines
(See ICLAC register)

MDA-MB-435 (SAMN03151832)

Animals and other research organisms

Policy information about studies involving animals; ARRIVE guidelines recommended for reporting animal research, and Sex and Gender in Research

Laboratory animals

female NOD.Cg-Prkdcscid Il2rgtm1Wjl/SzJ (NSG)-mice (8 to 12 weeks old) were purchased from Charles River, Sulzfeld.

Wild animals

Provide details on animals observed in or captured in the field; report species and age where possible. Describe how animals were caught and transported and what happened to captive animals after the study (if killed, explain why and describe method; if released, say where and when) OR state that the study did not involve wild animals.

Reporting on sex

Indicate if findings apply to only one sex; describe whether sex was considered in study design, methods used for assigning sex. Provide data disaggregated for sex where this information has been collected in the source data as appropriate; provide overall numbers in this Reporting Summary. Please state if this information has not been collected. Report sex-based analyses where performed, justify reasons for lack of sex-based analysis.

Field-collected samples

For laboratory work with field-collected samples, describe all relevant parameters such as housing, maintenance, temperature, photoperiod and end-of-experiment protocol OR state that the study did not involve samples collected from the field.

Ethics oversight

Animal studies were in compliance with German Cancer Center Institute guidelines and approved by the district government of lower Franconia (protocol number 55.2-2532-2-335) or governmental review board of the state of Baden-Wuerttemberg, Regierungspraesidium Karlsruhe, under the authorization number G-176/19, followed the German legal regulations. Experiments were conducted in accordance with the US National Institutes of Health Guide for the Care and Use of Laboratory Animals.

Note that full information on the approval of the study protocol must also be provided in the manuscript.

Dual use research of concern

Policy information about dual use research of concern

Hazards

Could the accidental, deliberate or reckless misuse of agents or technologies generated in the work, or the application of information presented in the manuscript, pose a threat to:

No	Yes	
☒	☐	Public health
☒	☐	National security
☒	☐	Crops and/or livestock
☒	☐	Ecosystems
☒	☐	Any other significant area

Experiments of concern

Does the work involve any of these experiments of concern:

No	Yes	
☒	☐	Demonstrate how to render a vaccine ineffective
☒	☐	Confer resistance to therapeutically useful antibiotics or antiviral agents
☒	☐	Enhance the virulence of a pathogen or render a nonpathogen virulent
☒	☐	Increase transmissibility of a pathogen
☒	☐	Alter the host range of a pathogen
☒	☐	Enable evasion of diagnostic/detection modalities
☒	☐	Enable the weaponization of a biological agent or toxin
☒	☐	Any other potentially harmful combination of experiments and agents

Flow Cytometry

Plots

Confirm that:

☒ The axis labels state the marker and fluorochrome used (e.g. CD4-FITC).

☒ The axis scales are clearly visible. Include numbers along axes only for bottom left plot of group (a 'group' is an analysis of identical markers).

☒ All plots are contour plots with outliers or pseudocolor plots.

☒ A numerical value for number of cells or percentage (with statistics) is provided.

Methodology

Sample preparation	100,000 cells per well were seeded on 6-well dishes (Sarstedt) one day prior to the experiment in the presence of the tested lipid. On the next day, cells were washed and treated with the indicated concentration of RSL3 to induce ferroptosis. Cells were subsequently incubated with C11-BODIPY (581/591) (1 µM) for 20 min at 37°C before they were harvested by trypsinisation. Subsequently, cells were resuspended in 500 µL of fresh PBS (DPBS, Gibco) and analysed using an excitation of 488-nm (FACS Canto II, BD Biosciences). Data was collected from the FL1 detector (C11-BODIPY) with a 502LP and 530/30 BP filter. At least 10,000 events were analysed per sample. Data was analysed using FlowJo Software.
Instrument	FACS Canto II
Software	For data collection the BF Bioscience was used. For data analysis Flowing software was used.
Cell population abundance	The abundance of the desired cell population in post-sort fractions was generally > 96% of the total post-sort population.
Gating strategy	Live cell population were separated from cellular debris and dead cells using FSC/SSC.

☒ Tick this box to confirm that a figure exemplifying the gating strategy is provided in the Supplementary Information.